


Srebp-controlled glucose metabolism is essential for NK cell functional responses

Nadine Assmann¹, Katie L O'Brien^{1,4}, Raymond P Donnelly^{1,4}, Lydia Dyck¹, Vanessa Zaiatz-Bittencourt¹, Róisín M Loftus¹, Paul Heinrich², Peter J Oefner², Lydia Lynch¹, Clair M Gardiner¹, Katja Dettmer² & David K Finlay^{1,3} 

Activated natural killer (NK) cells engage in a robust metabolic response that is required for normal effector function. Using genetic, pharmacological and metabolic analyses, we demonstrated an essential role for Srebp transcription factors in cytokine-induced metabolic reprogramming of NK cells that was independent of their conventional role in the control of lipid synthesis. Srebp was required for elevated glycolysis and oxidative phosphorylation and promoted a distinct metabolic pathway configuration in which glucose was metabolized to cytosolic citrate via the citrate–malate shuttle. Preventing the activation of Srebp or direct inhibition of the citrate–malate shuttle inhibited production of interferon- γ and NK cell cytotoxicity. Thus, Srebp controls glucose metabolism in NK cells, and this Srebp-dependent regulation is critical for NK cell effector function.

Cellular metabolism is now recognized as an important factor that can determine the fate and function of lymphocytes¹. Different lymphocyte subsets have distinct metabolic phenotypes that match the particular requirements of that cell². Additionally, certain metabolic regulators, metabolic enzymes and even metabolites have been shown to have direct immunoregulatory roles². The characterization of this metabolic immunoregulatory axis has revealed various novel therapeutic strategies with which to alter the course of lymphocyte responses³.

Natural killer (NK) cells are lymphocytes with important functions in anti-tumor and anti-viral responses⁴. NK cell responses are often found to be dysfunctional not only in chronic inflammatory diseases such as chronic viral infection and cancer but also in patients with obesity, which is also associated with chronic inflammation^{5–9}. The NK cell defects observed in obese people probably contribute to the increased incidence of cancer and risk of viral infection in these patients^{10,11}. While traditionally classified as innate lymphocytes, in fact NK cells have important functions both early, during the innate phase of the immune response, and later, alongside T lymphocytes and B lymphocytes, during the adaptive response. Metabolic reprogramming is required in cytokine-stimulated NK cells for their optimal function. NK cells that cannot maintain elevated rates of glycolysis or oxidative phosphorylation (OxPhos) have impaired effector responses^{12,13}.

Activated lymphocytes take up large amounts of glucose and have high rates of glycolysis to fuel various biosynthetic pathways; for example, they can produce serine (important for nucleotide and phospholipid synthesis) and fatty acids (important for lipid synthesis). Lipid-synthesis pathways are important during the metabolic reprogramming of effector T lymphocytes^{14,15}. Members of the Srebp

family of transcription factors are considered the master regulators of *de novo* lipid synthesis. In mammals, there are two genes that encode Srebp1 and Srebp2, which promote the expression of genes involved in fatty-acid synthesis and cholesterol synthesis, respectively. Additionally, Srebp transcription factors also regulate genes encoding molecules involved in the pentose phosphate pathway (PPP) that produces NADPH, an important reducing equivalent for anabolic processes, including lipid synthesis and nucleotide synthesis^{16,17}. Disrupting Srebp signaling or disrupting lipid synthesis inhibits the formation of effector T cell subsets, CD8⁺ cytotoxic T lymphocytes (CTLs) and the CD4⁺ T_H17 subset of helper T cells, respectively^{14,15}. The influence of Srebp transcription factors and *de novo* lipid-synthesis pathways on the metabolic and functional responses of NK cells is not known. As glucose can be a key fuel for *de novo* lipid synthesis following metabolism via glycolysis, we considered whether the functional defects we observed in NK cells with impaired glucose metabolism were due, at least in part, to defects in lipid synthesis^{12,13}.

Here we found that cytokine-stimulated NK cells upregulated Srebp signaling and lipid-synthesis pathways. Srebp activity was crucial for the growth, proliferation and effector function of NK cells, but lipid synthesis was not. We demonstrated that Srebp activity was essential for the metabolic reprogramming of NK cells and for the attainment of elevated glycolysis and OxPhos.

RESULTS

Srebp controls cytokine-induced growth and proliferation

Glucose metabolism through glycolysis is essential for the increased cellular growth of NK cells stimulated with interleukin 2 (IL-2) and IL-12 (called 'cytokine stimulation' here, unless specified otherwise), which

¹School of Biochemistry and Immunology, Trinity Biomedical Sciences Institute, Trinity College Dublin, Ireland. ²Institute of Functional Genomics, University of Regensburg, Regensburg, Germany. ³School of Pharmacy and Pharmaceutical Sciences, Trinity Biomedical Sciences Institute, Trinity College Dublin, Ireland. ⁴These authors contributed equally to this work. Correspondence should be addressed to D.K.F. (finlayd@tcd.ie).

Received 22 December 2016; accepted 18 August 2017; published online 18 September 2017; doi:10.1038/ni.3838

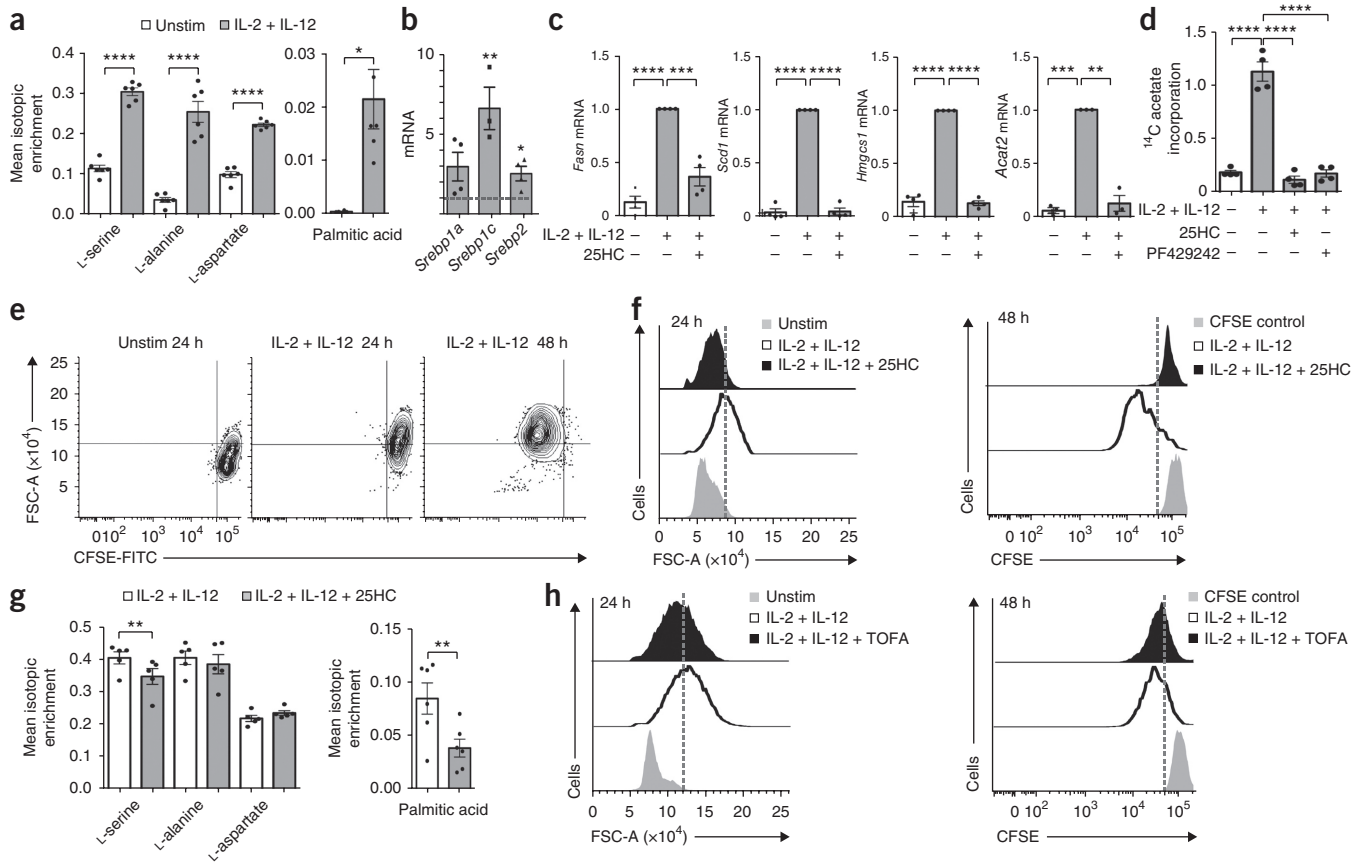


Figure 1 Srebp transcription factors are required for cytokine-induced NK cell growth and proliferation. **(a)** Incorporation of the ^{13}C label into amino acids (left) and palmitic acid (right) in NK cells left unstimulated (Unstim) or stimulated for 18 h with IL-2 plus IL-12 (key) in medium containing $^{13}\text{C}_6$ -glucose. **(b,c)** qRT-PCR analysis of *Srebp1* mRNA (*Srebp1a* and *Srebp1c* splice variants) and *Srebp2* mRNA **(b)** or of *Fasn*, *Scd1*, *Hmgcs1* and *Acat2* mRNA **(c)** in NK cells stimulated as in **a** alone **(b)** or in the presence (+) or absence (-) of 25HC (grid below **c**); results are presented relative to those of unstimulated cells **(b)** or cells stimulated with IL-2 plus IL-12 without 25HC **(c)**. **(d)** Incorporation of ^{14}C -acetate (nmol per 1×10^6 cells) into cellular lipids in NK cells stimulated as in **a** in the presence or absence of 25HC or PF429242 (grid below plot) in medium containing $^{14}\text{C}_2$ -acetate. **(e,f)** Flow cytometry of NK cells stained with the division-tracking dye CFSE and left unstimulated for 24 h or stimulated for 24 h or 48 h with IL-2 plus IL-12 (above plots **e**) in the presence or absence of 25HC (key **f**), assessing size (as forward scatter (FSC-A)) and proliferation (as CFSE dilution). CFSE control, cells stimulated for 24 h with IL-2 plus IL-12. **(g)** Incorporation of ^{13}C label as in **a** in NK cells stimulated as in **a** in the presence or absence of 25HC (key). **(h)** Flow cytometry as in **f** of CFSE-stained NK cells stimulated as in **e,f** in the presence or absence of TOFA (key). * $P < 0.05$, ** $P < 0.01$, *** $P < 0.001$ and **** $P < 0.0001$ (one-way analysis of variance (ANOVA) with the Sidak post-test **(a, left)** or Tukey post-test **(d)**, paired two-tailed t -test **(a, right, g)** or one-sample t -test **(b,c)**). Data are from six experiments **(a)**, three to four experiments **(b,c)**, four experiments **(d)** or five to six experiments **(g)**; mean + s.e.m. in each) or are representative of five experiments **(e,f,h)**.

indicates that glucose is important for cellular biosynthesis (ref. 12). ^{13}C -glucose-tracing metabolomics demonstrated that after 18 h of cytokine stimulation, NK cells used glucose to fuel the biosynthesis of amino acids and fatty acids (Fig. 1a). The incorporation of glucose into fatty acids was associated with increased expression of mRNA encoding the Srebp transcription factors that are the master regulators of lipid-synthesis pathways¹⁸ (Fig. 1b). The expression of Srebp target genes encoding molecules important for *de novo* fatty-acid synthesis (fatty-acid synthase (*Fasn*) and stearyl-coenzyme A (CoA) desaturase 1 (*Scd1*)) and those encoding molecules in the mevalonate pathway that is used to synthesize cholesterol (3-hydroxy-3-methylglutaryl-CoA synthase 1 (*Hmgcs1*) and acetyl-CoA acetyltransferase 2 (*Acat2*)) were robustly induced following 18 h of cytokine stimulation (Fig. 1c). Two separate pharmacological strategies were used to inhibit the activation of Srebp in cytokine-stimulated NK cells: 25-hydroxycholesterol (25HC) and PF429242, which act through distinct mechanisms to prevent the processing of a Srebp into an active transcription factor^{19,20} (Supplementary Fig. 1a). 25HC and PF429242 prevented

the upregulation of Srebp target genes in response to cytokine stimulation (Fig. 1c and Supplementary Fig. 1b). Additionally, cytokine-stimulated NK cells increased their rate of lipid synthesis, and this increase was blocked by both 25HC and PF429242 (Fig. 1d). The metabolic checkpoint kinase complex mTORC1 has been shown to regulate numerous steps in the Srebp-activation process in other cell types²¹. The expression of Srebp target genes in cytokine-stimulated NK cells was significantly reduced by the mTORC1 inhibitor rapamycin (Supplementary Fig. 1c).

Cytokine-stimulated NK cells underwent robust cellular growth within the first 24 h after stimulation, which resulted in increased cell size, and then the NK cells started to proliferate (Fig. 1e and Supplementary Fig. 1d). Inhibition of Srebp with 25HC or PF429242 restricted both cytokine-stimulated growth and cytokine-stimulated proliferation (Fig. 1f and Supplementary Fig. 2a,b). The incorporation of $^{13}\text{C}_6$ -glucose into serine and into fatty acids was decreased in cytokine-stimulated NK cells in the presence of 25HC, consistent with decreased *de novo* lipid synthesis (Fig. 1d,g). To investigate whether

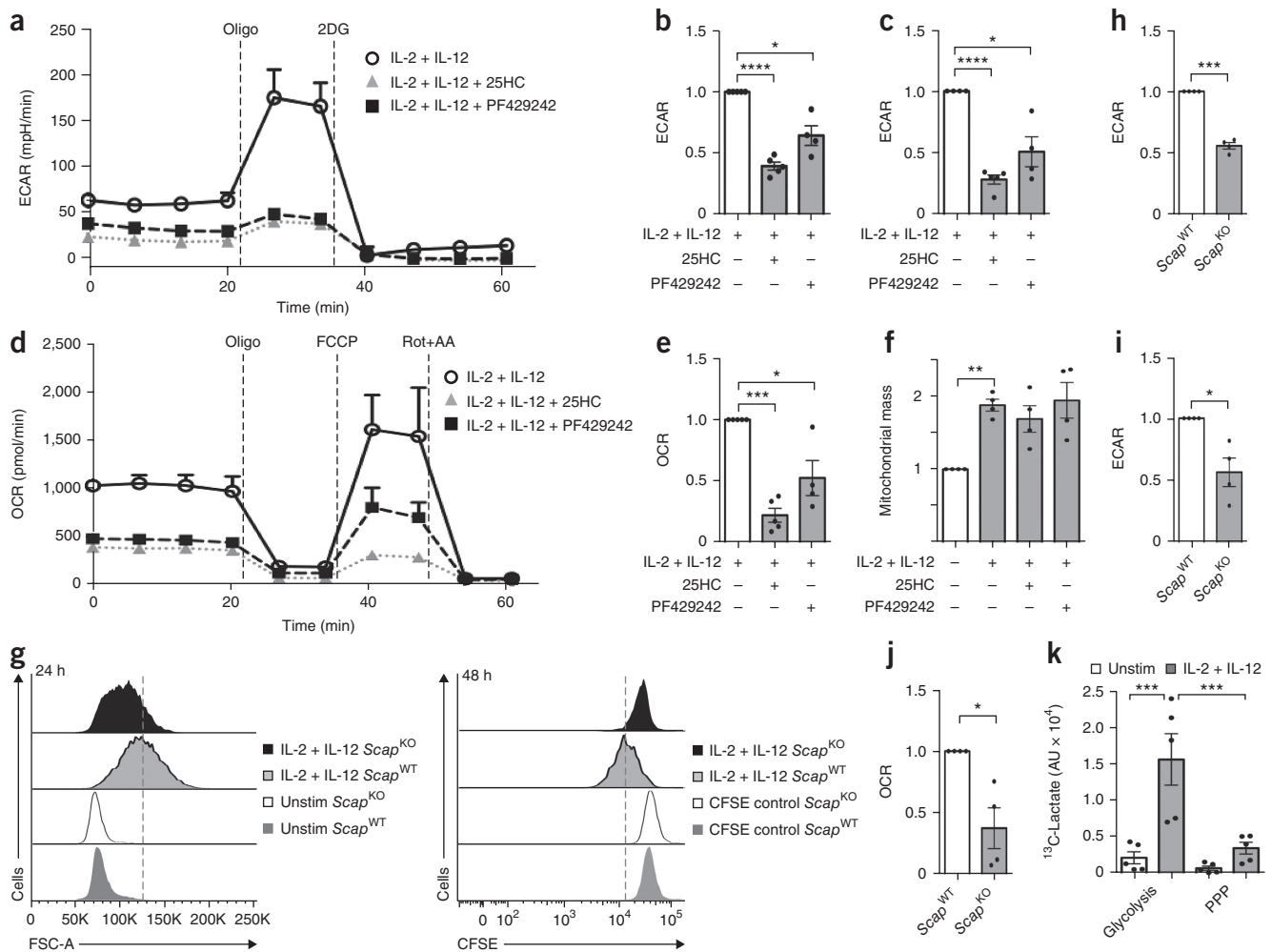


Figure 2 Srebp transcription factors are required for cytokine-induced glycolysis and OxPhos. (**a–e**) ECAR analysis (**a**) and ECAR (pooled data) of the glycolytic rate (**b**) and glycolytic capacity (**c**), as well as OCR analysis (**d**) and OCR (pooled data) (**e**) of NK cells stimulated for 18 h with IL-2 plus IL-12, in the presence or absence of 25HC and PF429242 (key (**a,d**) or grid below plot (**b,c,e**)), assessed with sequential injection (dashed vertical lines, **a,d**) of the mitochondrial ATP-synthase inhibitor oligomycin (Oligo) and the glucose analog 2-deoxyglucose (2DG) (**a–c**) or oligomycin, the mitochondrial uncoupler FCCP and inhibitors of the electron-transport-chain complex I and III, rotenone and antimycin A (Rot + AA) (**d,e**); results in **b,c,e** are presented relative to those of NK cells stimulated without inhibitors. (**f**) Mitochondrial mass of NK cells left unstimulated or stimulated as in **a–e** in the presence or absence of 25HC and PF429242 (grid below plot), assessed with a mitochondria-specific fluorescent dye; results are presented relative to those of unstimulated NK cells. (**g**) Flow cytometry (as in **Fig. 1f**) of CFSE-stained *Scap*^{KO} and *Scap*^{WT} NK cells stimulated for 24 h (left) or 48 h (right) with IL-2 plus IL-12. (**h–j**) ECAR of the glycolytic rate (**h**) and glycolytic capacity (**i**), and OCR (**j**), of *Scap*^{KO} and *Scap*^{WT} NK cells (horizontal axis) stimulated as in **a–e**; results are presented relative to those of *Scap*^{WT} cells (CFSE control, as in **Fig. 1f**). (**k**) ¹³C labeling of lactate in NK cells left unstimulated or stimulated for 18 h with IL-2 plus IL-12 in medium containing 1,2-¹³C₂-glucose, assessing the generation of lactate by glycolysis versus the PPP (horizontal axis); results are presented in arbitrary units (AU). **P* < 0.05, ***P* < 0.01, ****P* < 0.001 and *****P* < 0.0001 (one-sample *t*-test (**b,c,e,f,h–j**) or one-way ANOVA with the Tukey post-test (**k**)). Data are representative of four to five experiments (**a,d,g**) or are from four to five experiments (**b,c,e**), four experiments (**f,h,i,j**) or five experiments (**k**; mean + s.e.m. in each).

the observed defects in NK cell growth and proliferation were due to the loss of Srebp-dependent lipid synthesis, we used inhibitors that directly target *de-novo*-lipid-synthesis pathways. Inhibition of acetyl-CoA carboxylase, the first enzymatic step in the fatty-acid- and mevalonate-synthesis pathways, with TOFA (5-(tetradecyloxy)-2-furoic acid) or inhibition of fatty-acid synthase with C75 (4-methylene-2-octyl-5-oxotetrahydrofuran-3-carboxylic acid) had a minimal effect on NK cell growth and proliferation (**Fig. 1h** and **Supplementary Fig. 2b,c**). Inhibition of acetyl-CoA carboxylase (with TOFA) and inhibition of Srebp activation (with 25HC or PF429242) had equivalently small effects on the viability of cytokine-stimulated NK cells after 20 h (**Supplementary Fig. 2d**). We found that in contrast

to the proliferation of NK cells, the proliferation of CTLs in response to IL-2 was inhibited by PF429242, 25HC and TOFA (**Supplementary Fig. 2e,f**). Collectively, these findings supported the proposal of a role for Srebp transcription factors in sustaining the growth and proliferation of cytokine-stimulated NK cells, a function that was independent of their role in promoting lipid synthesis.

Cytokine-induced glycolysis and OxPhos require Srebp

We next considered explanations for those Srebp-dependent, lipid-synthesis-independent effects on the growth and proliferation of cytokine-stimulated NK cells. Cytokine stimulation induces elevated rates of glycolysis that are required for cytokine-induced NK cell

growth¹². Therefore, we considered whether Srebp activity might be required for the elevated glycolysis in cytokine-stimulated NK cells. NK cells stimulated with cytokines in the presence of 25HC or PF429242 had substantially lower glycolysis and glycolytic capacity than that of NK cells stimulated with cytokines in the absence of those inhibitors, as measured by the extracellular acidification rate (ECAR) (Fig. 2a–c and Supplementary Fig. 3a). In contrast, inhibition of acetyl-CoA carboxylase or fatty-acid synthase did not inhibit glycolysis in cytokine-stimulated NK cells (Supplementary Fig. 3b,c). NK cells stimulated with cytokines in the presence of 25HC or PF429242 also failed to upregulate OxPhos and had lower maximal respiration than that of NK cells stimulated with cytokines in the absence of those inhibitors, as measured by the oxygen-consumption rate (OCR) (Fig. 2d,e). The increased rate of OxPhos in cytokine-stimulated NK cells was associated with an increase in mitochondrial mass, as determined by staining with a mitochondria-specific fluorescent dye, but inhibition of Srebp did not affect this increase in mitochondrial abundance (Fig. 2f).

To further investigate Srebp's function in NK cells, we crossed mice with *loxP* sites flanking exon 1 of *Scap* (which encodes the Srebp-cleavage-activating protein SCAP) to mice expressing a tamoxifen-inducible Cre recombinase^{18,22}. The treatment of cultured NK cells with 4-hydroxytamoxifen resulted in the deletion of *Scap*, which prevented the activation of Srebp and the expression of Srebp target genes (Supplementary Fig. 3d). Unstimulated NK cells in which *Scap* was deleted (*Scap*^{KO}) were equivalent in size to NK cells with wild-type *Scap* (*Scap*^{WT}). However, following cytokine stimulation, *Scap*^{KO} NK cells proliferated less and were smaller than *Scap*^{WT} NK cells, consistent with the results of experiments using inhibitors of Srebp activation (25HC and PF429242) (Fig. 2g and Supplementary Fig. 3e). Cytokine-stimulated *Scap*^{KO} NK cells also had less glycolysis, glycolytic capacity and OxPhos than that of *Scap*^{WT} NK cells (Fig. 2h–j). Together these pharmacological and genetic data showed that cytokine-induced metabolic responses in NK cells were blocked in the absence of Srebp activity.

We next considered the potential mechanisms underpinning Srebp-regulated glycolysis in cytokine-stimulated NK cells. Although no link between Srebp and glycolysis has been reported, Srebp activity does influence the PPP that branches away from the glycolytic pathway at glucose-6-phosphate¹⁷. Glucose-6-phosphate dehydrogenase, the first enzyme in the PPP, is encoded by *G6pd*, which is a target of Srebp¹⁷. *G6pd* expression was induced in cytokine-stimulated NK cells and was inhibited when the activation of Srebp was prevented (Supplementary Fig. 4a). Lactate can also be produced when glucose is metabolized through the PPP. Thus, the lower ECAR measurements observed in NK cells in which Srebp was inhibited might have been due to less PPP-mediated glucose metabolism rather than to less glycolysis. To determine the route by which glucose was converted to lactate in the cytokine-stimulated NK cells, we performed metabolic tracing experiments using 1,2-¹³C₂-glucose (glucose labeled with ¹³C carbon atoms on positions 1 and 2) (Supplementary Fig. 4b). This approach showed that the majority of the lactate produced by cytokine-stimulated NK cells passed through glycolysis rather than through the PPP (Fig. 2k). Therefore, the lower ECAR values in NK cells in which Srebp was inhibited reflected decreased flux through glycolysis.

Srebp inhibition does not prevent mTORC1 signaling

It has been shown that mTORC1 signaling is required for the elevated glycolysis in cytokine-stimulated NK cells¹²; thus, we considered whether inhibition of Srebp might affect the activity of mTORC1,

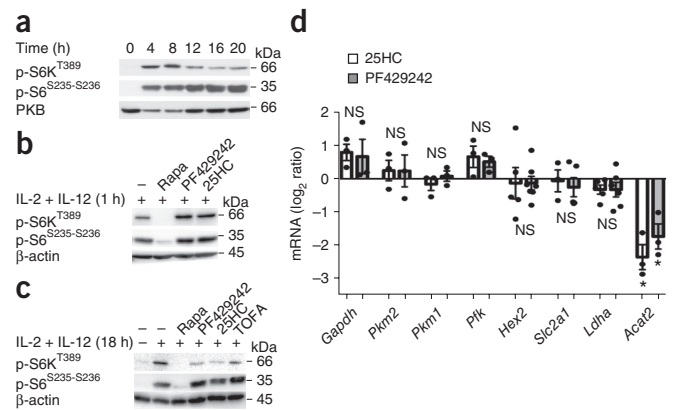


Figure 3 Inhibition of Srebp does not prevent mTORC1 signaling. (a–c) Immunoblot analysis of S6K phosphorylated at Thr389 (p-S6K^{T389}) and S6 phosphorylated at Ser235 and Ser236 (p-S6^{S235-S236}), as well as PKB or β -actin (loading controls), in NK cells left unstimulated or stimulated for 0–20 h (above lanes) with IL-2 plus IL-12 (a), or stimulated for 1 h (b) or 18 h (c) with IL-2 plus IL-12 in the presence or absence of 25HC, PF429242, TOFA or rapamycin (Rapa; control for inactive mTORC1) (above blots); right margin, molecular size, in kilodaltons (kDa). (d) qRT-PCR analysis of *Gapdh*, *Pkm2*, *Pkm1*, *Pfk*, *Hex2*, *Slc2a1* and *Ldha* mRNA, as well as *Acat2* mRNA (known Srebp target gene and positive control), in NK cells stimulated for 18 h with IL-2 plus IL-12 in the presence or absence of 25HC or PF429242 (key); results are presented as the ratio of IL-2 plus IL-12 with inhibitor to IL-2 plus IL-12. NS, not significant ($P > 0.05$); * $P < 0.05$ (one-sample *t*-test). Data are representative of three to four independent experiments (a–c) or three to seven independent experiments (d; mean + s.e.m.).

which can be monitored via phosphorylation of the mTORC1 substrate p70 S6 kinase (S6K) and the S6K substrate S6 ribosomal protein (S6). mTORC1 was activated throughout the entire duration of cytokine stimulation (Fig. 3a). Inhibition of Srebp did not affect initial mTORC1 signaling (at 1 h after stimulation) and resulted in only slightly less mTORC1 signaling observed at a later time point (18 h) (Fig. 3b,c). Rapamycin-mediated inhibition of mTORC1 activity prevents the increased expression of components of the glycolytic machinery, glucose transporters and glycolytic enzymes, associated with cytokine-induced metabolic reprogramming of NK cells¹². The small decrease in mTORC1 signaling observed following inhibition of Srebp activation with 25HC or PF429242 did not influence the expression of genes encoding those glycolytic enzymes or the glucose transporter *Slc2a1* (Fig. 3d). Inhibition of the fatty-acid- and mevalonate-synthesis pathways with TOFA had a small effect on mTORC1 signaling similar to that observed with 25HC or PF429242 but, notably, TOFA did not inhibit NK cell glycolysis (Fig. 3c and Supplementary Fig. 3b,c). Together these data indicated that diminished mTORC1 activity did not account for the metabolic defects observed in cytokine-stimulated NK cells lacking Srebp activity.

Glucose is metabolized to cytosolic citrate

To understand how Srebp was controlling mitochondrial metabolism, we performed metabolomics analysis of cytokine-stimulated NK cells. There was an increase in tricarboxylic acid (TCA)-cycle intermediates following cytokine stimulation, but there was a clear imbalance in this, with the concentration of citrate being significantly greater than that of the downstream TCA-cycle intermediates succinate and fumarate (Fig. 4a). Metabolic-tracing analysis with uniformly labeled ¹³C₆-glucose (all six carbon atoms labeled) was used to acquire additional information on how glucose was used in the cytokine-stimulated

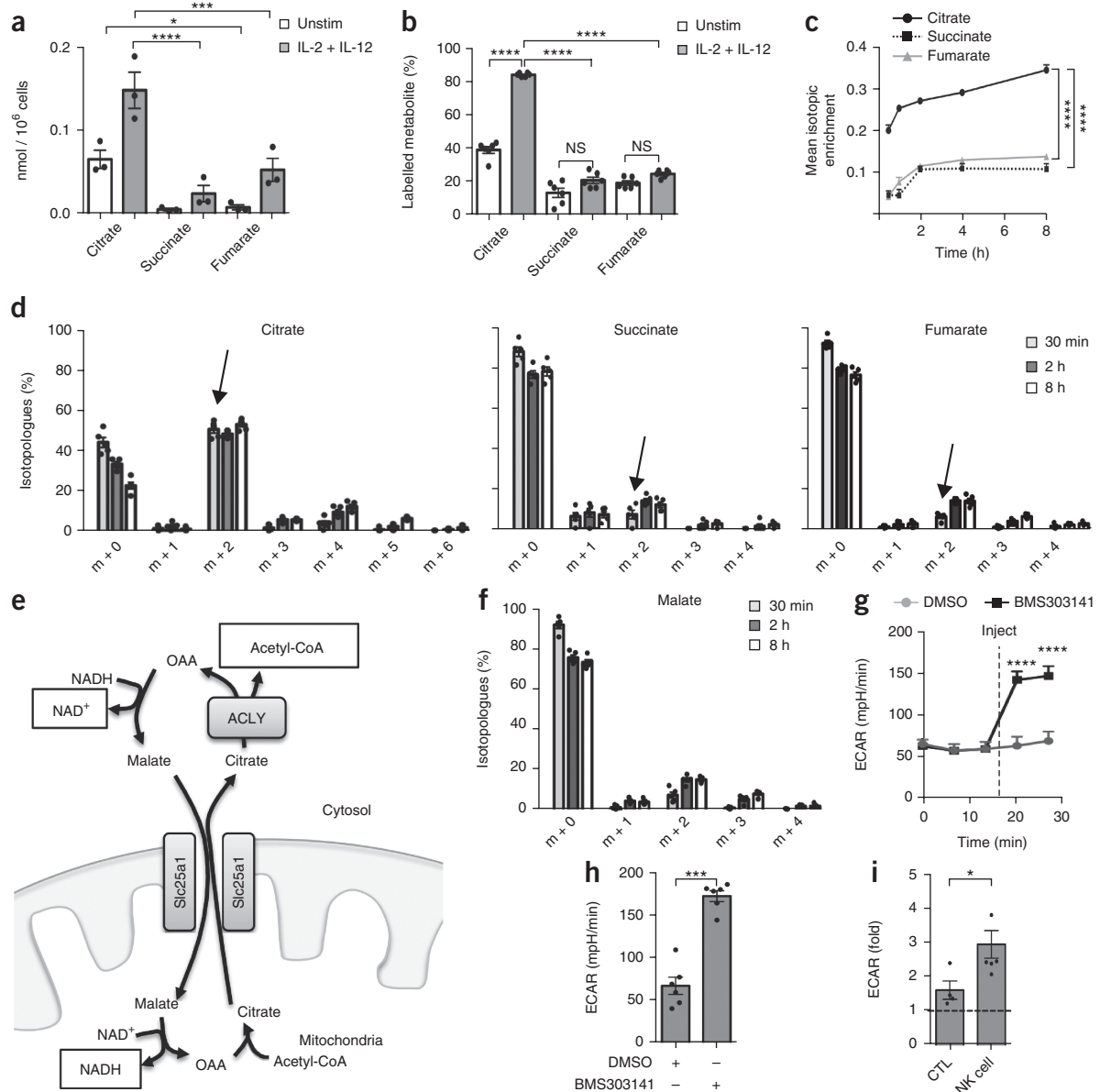


Figure 4 Glucose is metabolized to cytosolic citrate in cytokine activated NK cells. **(a)** Liquid chromatography–tandem mass spectrometry analysis of citrate, succinate and fumarate in NK cells left unstimulated or stimulated for 18 h with IL-2 plus IL-12 (key). **(b)** Incorporation of ^{13}C into citrate, succinate and fumarate in NK cells stimulated as in **a** in medium containing $^{13}\text{C}_6$ -glucose, assessed by metabolic tracing. **(c,d,f)** Incorporation of the ^{13}C label into citrate, succinate and fumarate **(c)** and the isotopologue distribution for citrate, succinate, fumarate **(d)** and malate **(f)** in NK cells stimulated as in **a** with unlabeled glucose and pulsed for up to 8 h (horizontal axis **(c)** or key **(d,f)**) with medium containing $^{13}\text{C}_6$ -glucose; arrows in **d** show citrate molecules with two ^{13}C atoms in cells pulsed for 30 min. **(e)** The citrate–malate shuttle, showing the main outputs of the citrate–malate shuttle: cytosolic NAD^+ , cytosolic acetyl-CoA and mitochondrial NADH . **(g,h)** ECAR in NK cells stimulated as in **a**, analyzed before and after injection of the vehicle DMSO or BMS303141 **(g)**, and pooled results as in **g** obtained at the second measurement after injection **(h)**. **(i)** ECAR of CTLs cultured with IL-2 and in NK cells stimulated as in **a** (horizontal axis), analyzed after injection of DMSO or BMS303141 (second measurement after injection); results are presented relative to those of DMSO-treated cells. * $P < 0.05$, *** $P < 0.001$ and **** $P < 0.0001$ (two-way ANOVA with the Sidak post-test **(a,b,c,g)** or paired **(h)** or unpaired **(i)** two-tailed t -test). Data are from three **(a)**, six **(b,h)**, five **(c,d,f)** or four to six **(i)** independent experiments (mean + s.e.m. in each) or are representative of six independent experiments **(g; mean + s.e.m.)**.

NK cells. While these analyses did not quantitatively account for all the labeled metabolites, the pattern of incorporation of ^{13}C into the various metabolites and the distribution of isotopologues within individual metabolites was informative. These experiments revealed a large increase in the metabolism of glucose to citrate in cytokine-stimulated NK cells; >80% of the citrate contained ^{13}C atoms (**Fig. 4b** and **Supplementary Fig. 5a**). In contrast, succinate and fumarate

contained predominantly unlabeled carbon from sources other than glucose (**Fig. 4b**). Therefore, glucose was a key fuel for generating citrate in cytokine-stimulated NK cells, but those glucose-derived carbon atoms were not passed downstream within the TCA cycle.

Mitochondrial citrate can also be exported into the cytosol, where it can be further metabolized to feed into a range of metabolic and biosynthetic pathways. To investigate whether glucose was being used

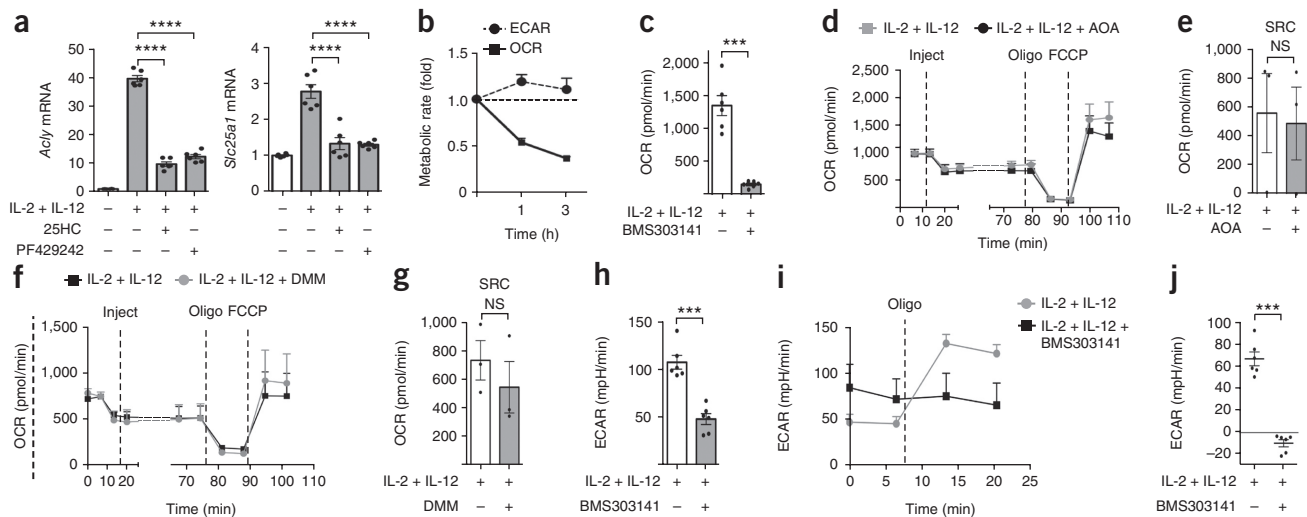


Figure 5 Cytosolic citrate metabolism is needed to sustain elevated OxPhos and glycolysis. **(a)** qRT-PCR analysis of *Acly* and *Slc25a1* mRNA in NK cells left unstimulated or stimulated for 18 h with IL-2 plus IL-12 in the presence or absence of 25HC or PF429242 (grid below plot); results are presented relative to those of unstimulated NK cells. **(b)** Metabolic rate of NK cells stimulated as in **a** and treated for 1 h or 3 h (horizontal axis) with DMSO or BMS303141; results are presented relative to those of DMSO-treated cells. **(c)** OCR of NK cells stimulated as in **a**, then incubated for 3 h in medium containing BMS303141 (+) or DMSO (-), assessed after the addition of FCCP. **(d,f)** OCR of NK cells stimulated as in **a** following the sequential injection of aminoxyacetic acid (AOA) (**d**) or dimethyl malonate (DMM) (**f**) or medium (far left), oligomycin and FCCP (dashed vertical lines). **(e,g)** OCR (after the addition of FCCP) and spare respiratory capacity (SRC) of NK cells stimulated as in **d** (**e**) or **f** (**g**). **(h-j)** ECAR of NK cells stimulated as in **a** and treated for 3 h with BMS303141 or DMSO, assessed before and after the addition of oligomycin (**i**), and calculated values for the glycolytic capacity (**h**) and glycolytic reserve (**j**) (both pooled data). * $P < 0.05$, *** $P < 0.001$ and **** $P < 0.0001$ (one-way ANOVA with the Tukey post-test (**a**), one-sample t -test (**b**) or paired two-tailed t -test (**c,e,g,h,j**)). Data are from six experiments (**a,c,h,j**), six to seven experiments (**b**) or three experiments (**e,g**; mean + s.e.m. in each) or are representative of three experiments (**d,f**) or six experiments (**i**; mean + s.e.m. in each).

to generate cytosolic citrate, we pulsed cytokine-stimulated NK cells for 30 min to 8 h with medium containing $^{13}\text{C}_6$ -glucose. Citrate had a significantly greater mean isotopic enrichment than that of succinate or fumarate over the 8 h analyzed (**Fig. 4c**). The isotopologue distribution of the ^{13}C atoms within citrate, succinate and fumarate was then analyzed. Our prediction was that if glucose were metabolized mainly to cytosolic citrate, then 'm+2' labeled citrate (containing two ^{13}C atoms) would be observed, but succinate and fumarate would be predominantly 'm+0' (would contain no ^{13}C atoms) (**Supplementary Fig. 5b**). Alternatively, if glucose-derived citrate fed mainly into the TCA cycle, then m+2 citrate, m+2 succinate and m+2 fumarate would all be equally present (**Supplementary Fig. 5b**). The data from this experiment clearly showed substantial enrichment for m+2 citrate at 30 min; 50% of citrate molecules contained two ^{13}C carbon atoms (**Fig. 4d**). In contrast, the majority of succinate and fumarate were m+0 labeled, with only ~5% of isotopologues m+2 labeled (**Fig. 4d**). These isotopologue-distribution patterns did not change significantly over the 8 h analyzed (**Fig. 4d**). These data demonstrated that glucose was metabolized to cytosolic citrate in the cytokine-stimulated NK cells.

In the cytosol, citrate can be cleaved by ATP-citrate lyase (ACLY) to produce oxaloacetate and cytosolic acetyl-CoA, which is used for lipid synthesis and as a substrate for acetylation reactions (**Fig. 4e**). As the mitochondrial citrate transporter *Slc25a1* is an obligate citrate-malate antiporter, continued citrate export requires continued malate import (**Fig. 4e**). When ACLY cleaves m+2 citrate, the ^{13}C -labeled carbons are passed to cytosolic acetyl-CoA rather than to oxaloacetate²³. Therefore, the malate generated by the citrate-malate shuttle would be predicted to be predominantly the m+0 isotopologue, as was found to be the case (**Fig. 4f**).

If mitochondrial pyruvate were metabolized mainly to cytosolic acetyl-CoA and oxaloacetate, then inhibition of ACLY would disrupt the

use of pyruvate in the mitochondria, which would lead to the accumulation of cytosolic pyruvate and, as a result, the metabolism of pyruvate into lactate. Therefore, to further investigate mitochondrial metabolism, we monitored ECAR values (as a measure of lactate production) in cytokine-stimulated NK cells immediately following the addition of an ACLY inhibitor, BMS303141. There was an immediate increase in ECAR in response to the administration of BMS303141 (**Fig. 4g,h**), which demonstrated that cytosolic citrate metabolism via ACLY was important for mitochondrial pyruvate metabolism. Similar results were obtained with a separate inhibitor of ACLY, SB204990 (**Supplementary Fig. 5c**). In contrast, smaller increases in ECAR were observed in CTLs treated with BMS303141 or SB204990 than in their NK cell counterparts (**Fig. 4i** and **Supplementary Fig. 5d-f**). Collectively, these data showed that a major metabolic pathway in the cytokine-stimulated NK cells was the conversion of glucose into cytosolic citrate.

ACLY activity sustains elevated OxPhos and glycolysis

There are two outputs of the citrate-malate shuttle: electrons from cytosolic NADH pool are transferred to mitochondrial NADH to feed into OxPhos, and acetyl-CoA is generated in the cytosol²⁴ (**Fig. 4e**). Another important consequence of the citrate-malate shuttle is the regeneration of cytosolic NAD^+ , which is an essential cofactor for the glycolytic enzyme GAPDH (**Fig. 4e**). Genes encoding two of the key components of the citrate-malate shuttle, the citrate-malate antiporter *Slc25a1* and ACLY, have been described as Srebp1 targets in other cell types^{16,25-29}. Therefore, we considered whether Srebp-dependent OxPhos was due to Srebp-controlled expression of key components of the citrate-malate shuttle. The expression of *Acly* mRNA and *Slc25a1* mRNA was robustly increased in cytokine-stimulated NK cells, and those increases were substantially inhibited by both 25HC and PF429242 (**Fig. 5a**).

To determine if the Srebp-regulated citrate–malate shuttle was important in sustaining the elevated metabolic phenotype of cytokine-stimulated NK cells, we measured ECAR and OCR values 1 and 3 h following the addition of BMS303141. There was a

substantial decrease in the rate of OxPhos at 1 h after the addition of BMS303141, with a further decrease observed after 3 h (Fig. 5b). In contrast, there was no decrease in the glycolytic rate over this time period (Fig. 5b). Maximum respiration values were also substantially

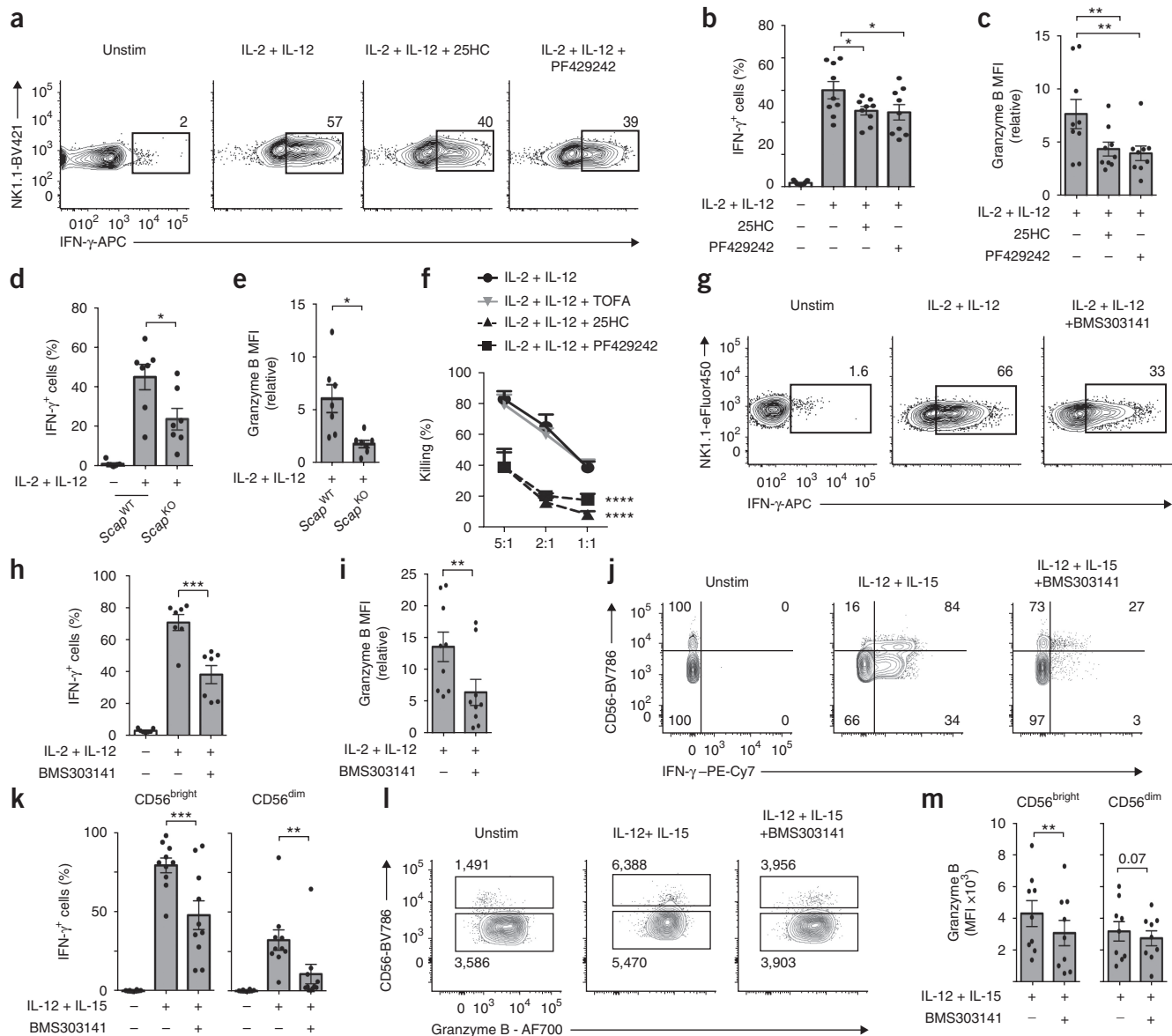


Figure 6 The Srebp-controlled citrate–malate shuttle is required for NK cell effector function. (**a–c**) Flow-cytometry analysis of the production of IFN- γ (**a**), the frequency of IFN- γ ⁺ cells (**b**) and expression of granzyme B (**c**) in NK cells left unstimulated or stimulated for 20 h with IL-2 plus IL-12 in the presence or absence of 25HC or PF429242; the mean fluorescence intensity (MFI) of granzyme B (**c**) is presented relative to that of unstimulated cells. Numbers adjacent to outlined areas (**a**) indicate percent IFN- γ ⁺ cells. (**d,e**) Flow-cytometry analysis of the frequency of IFN- γ ⁺ cells (**d**) and expression of granzyme B (**e**) in *Scap*^{KO} and *Scap*^{WT} NK cells (below plots) left unstimulated or stimulated for 20 h with IL-2 plus IL-12; granzyme B expression is presented relative to that of unstimulated *Scap*^{WT} cells. (**f**) Cytotoxicity of NK cells left unstimulated or stimulated for 18 h with IL-2 plus IL-12 in the presence or absence of 25HC, PF429242 or TOFA (key) and incubated for 4 h with tumor target cells (ratio (effector:target), horizontal axis), presented as the proportion of target cells killed (Killing (%)). (**g–i**) Flow-cytometry analysis of the production of IFN- γ (**g**), the frequency of IFN- γ ⁺ cells (**h**) and expression of granzyme B (**i**) in NK cells stimulated as in **a–c** in the presence or absence of BMS303141 (numbers adjacent to outlined areas (**g**) as in **a**; granzyme B expression (**i**) as in **c**). (**j–m**) Flow-cytometry analysis of the production of IFN- γ (**j**), the frequency of IFN- γ ⁺ cells (**k**) and the expression of granzyme B (**l,m**) in human NK cells left unstimulated or stimulated for 18 h with IL-12 plus IL-15 in the presence or absence of BMS303141. Numbers in quadrants (**j**) indicate percent CD56^{bright} cells that produce IFN- γ (top right) or not (top left) or CD56^{dim} cells that produce IFN- γ (bottom right) or not (bottom left); numbers in outlined areas (**l**) indicate mean fluorescence intensity of granzyme B in CD56^{bright} cells (top) or CD56^{dim} cells (bottom). * $P < 0.05$, ** $P < 0.01$, *** $P < 0.001$ and **** $P < 0.0001$ (one-way ANOVA with the Tukey post-test (**b–d,h**) or the Holm-Sidak post-test (**k**), two-way ANOVA with the Sidak post-test (**f**) or paired two-tailed *t*-test (**e,i,m**)). Data are representative of nine experiments (**a,l**), seven experiments (**g**) or ten experiments (**j**) or are from nine experiments (**b,c,i,m**), seven experiments (**d,e,h**), three experiments (**f**) or ten experiments (**k**; mean + s.e.m. in each).

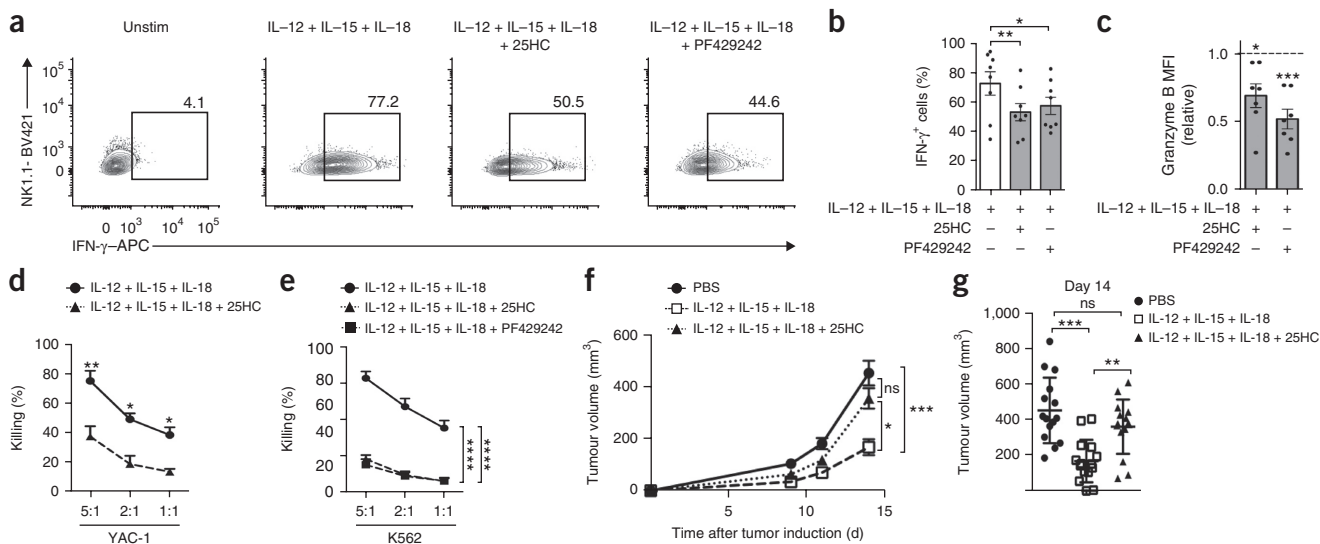


Figure 7 Srebp activity is important for therapeutic NK cell anti-tumor responses *in vivo*. (**a–c**) Flow-cytometry analysis of the production of IFN- γ (**a**), the frequency of IFN- γ ⁺ cells (**b**) and expression of granzyme B (**c**) in NK cells left unstimulated or stimulated for 20 h with IL-12 plus IL-15 plus IL-18 in the presence or absence of 25HC or PF429242; granzyme B expression (**c**) is presented relative to that in cells not treated with inhibitor. Numbers adjacent to outlined areas (**a**) indicate percent IFN- γ ⁺ cells. (**d,e**) Cytotoxicity of mouse NK cells stimulated for 18 h as in **a–c** in the presence or absence of 25HC or PF429242 (key) and incubated with YAC-1 tumor cells (**d**) or K562 human chronic myelogenous leukemia tumor cells (**e**) (ratio (effector:target), horizontal axis), presented as the proportion of target cells killed (Killing (%)). (**f,g**) Volume of tumors from C57BL/6 mice given injection of B16 tumor cells (into the flanks) on day 0, followed by injection, on days 3, 7 and 10, of PBS or NK cells that had been stimulated *in vitro* for 18 h as in **a–c** in the presence or absence of 25HC, analyzed on days 9, 11 and 14 (horizontal axis) (**f**) and on day 14 (**g**). Each symbol (**g**) represents an individual mouse; small horizontal lines indicate the mean \pm s.e.m. * $P < 0.05$, ** $P < 0.01$, *** $P < 0.001$ and **** $P < 0.0001$ (one-way ANOVA with the Tukey post-test (**b**), two-way ANOVA with the Tukey post-test (**f,g**) or Sidak post-test (**d,e**) or one-sample *t*-test (**c**). Data are representative of eight experiments (**a**), are from eight (**b**), seven (**c**), five (**d**) or four (**e**) experiments (mean \pm s.e.m. in each) or are pooled from two independent experiments (**f,g**; mean \pm s.e.m. of 15 total mice per group (**f**)).

decreased following treatment with BMS303141 (**Fig. 5c**). These data indicated that cytosolic NADH generated by glycolysis was essential for sustaining OxPhos via the citrate–malate shuttle. The function of transferring electrons between cytosolic and mitochondrial NAD pools is more commonly ascribed to the malate–aspartate shuttle than to the citrate–malate shuttle. However, in activated NK cells, an inhibitor of the malate–aspartate shuttle, aminooxyacetic acid, had no effect on the rate of OxPhos or the spare respiratory capacity (**Fig. 5d,e** and **Supplementary Fig. 3a**). Direct inhibition of the TCA-cycle enzyme succinate dehydrogenase with dimethyl-malonate did not significantly affect OxPhos or the spare respiratory capacity of cytokine-stimulated NK cells (**Fig. 5f,g** and **Supplementary Fig. 3a**). Together these data showed that the cytokine-stimulated NK cells maintained their elevated OxPhos via the glucose-dependent citrate–malate shuttle.

While initial analysis showed that BMS303141 did not inhibit basal ECAR values, further analysis showed that the glycolytic capacity of these cells was substantially decreased (**Fig. 5h**). BMS303141-treated NK cells fail to increase their ECAR values following the addition of oligomycin (**Fig. 5i,j** and **Supplementary Fig. 3a**), which indicated these cells were operating at a maximal glycolytic rate and had no appreciable glycolytic reserve. Indeed, increasing glycolytic flux to the maximal rate possible is the expected response for cells in which OxPhos and mitochondrial ATP production is severely compromised. These data revealed an essential role for ACLY activity in sustaining the metabolic phenotype of the cytokine-stimulated NK cells.

Srebp and the citrate–malate shuttle control NK cell function

NK cell metabolism is important for the effector function of both mouse NK cells and human NK cells^{12,13}. With that in mind, we investigated the effect of failed metabolism, due to the loss of Srebp activity, on the effector

function of NK cells. Preventing the activation of Srebp with 25HC or PF429242 inhibited the cytokine-induced production of interferon- γ (IFN- γ) and expression of granzyme B (**Fig. 6a–c**). Similarly, cytokine-stimulated *Scap*^{KO} NK cells showed less IFN- γ production and lower expression of granzyme B than that of cytokine-stimulated *Scap*^{WT} NK cells (**Fig. 6d,e**). In contrast, direct inhibition of lipid-synthesis pathways had no effect on the IFN- γ production or granzyme B expression of cytokine-stimulated NK cells, consistent with the finding that these inhibitors did not disrupt NK cell metabolism (**Supplementary Fig. 6a,b**). Additionally, 25HC and PF429242 significantly inhibited the cytotoxic effect of NK cells on target cells (YAC-1 cells derived from a mouse T cell lymphoma tumor), but TOFA did not (**Fig. 6f**).

Next we assessed the effect of direct inhibition of ACLY on NK cell function. Cytokine-stimulated NK cells treated with BMS303141 produced less IFN- γ and had lower expression of granzyme B than that of untreated NK cells (**Fig. 6g–i**). We further explored the importance of ACLY in NK cell responses in CD56^{dim} and CD56^{bright} NK cell subsets in peripheral blood mononuclear cells isolated from the blood of healthy donors. Published work has suggested that the CD56^{bright} subset engages in a more robust metabolic response following IL-12–IL-15 cytokine stimulation than does the CD56^{dim} subset¹³. BMS303141 strongly inhibited IFN- γ production induced by IL-12–IL-15 in both CD56^{dim} NK cells and CD56^{bright} NK cells and inhibited the expression of granzyme B in CD56^{bright} NK cells (**Fig. 6j–m** and **Supplementary Fig. 6c**). 25HC and PF429242 also diminished the IFN- γ production and granzyme B expression induced by IL-12–IL-15 in CD56^{bright} NK cells (**Supplementary Fig. 6d–g**). Together these data have identified a previously unknown Srebp-dependent metabolic circuit in cytokine-stimulated NK cells that was essential for normal NK cell function.

Srebp controls NK cell anti-tumor responses *in vivo*

Various approaches are being developed to utilize NK cells therapeutically to treat cancer. One such approach involves the adoptive transfer of NK cells stimulated with cytokine(s) *in vitro*³⁰. The combination of IL-12, IL-15 and IL-18 is becoming the standard stimulation protocol, as it sustains robust anti-tumor responses^{30,31}. With that in mind, we investigated whether Srebp signaling was important for the therapeutic anti-tumor effects of NK cells stimulated with IL-12–IL-15–IL-18 and then adoptively transferred, in the B16 mouse model of melanoma. *In vitro* IFN- γ production and granzyme B expression by NK cells stimulated with IL-12–IL-15–IL-18 was substantially reduced by treatment with 25HC or PF429242 (Fig. 7a–c). Additionally, NK cell-directed killing of tumor target cells was severely inhibited by both 25HC and PF429242, as measured by *in vitro* cytotoxicity assays (Fig. 7d,e).

The anti-tumor actions of NK cells stimulated with IL-12–IL-15–IL-18 were then investigated *in vivo*. B16 tumor cells were injected into the flanks of C57BL/6 mice on day 0, followed by the injection of *in vitro*-stimulated NK cells on days 3, 7 and 10 at the site of the tumor. The injection of NK cells stimulated with IL-12–IL-15–IL-18 significantly slowed the rate of tumor growth, relative to that of control mice that received injection of PBS (Fig. 7f,g). However, that therapeutic effect was lost when mice received NK cells stimulated with IL-12–IL-15–IL-18 in the presence 25HC; in these mice, tumor growth was similar to that of the control mice (Fig. 7f,g). Collectively, this study has shown that Srebp activity in NK cells was required for their acquisition of a metabolic phenotype that facilitated NK cell anti-tumor responses (Supplementary Fig. 7).

DISCUSSION

This study has discovered a previously unknown and unexpected role for Srebp transcription factors in NK cells as essential regulators of glucose metabolism. In contrast, Srebp-controlled lipid-synthesis pathways were not important for NK cell responses. The role of Srebp transcription factors in CD8⁺ T cells stimulated via the T cell antigen receptor has been investigated previously. CD8⁺ T cells that lack *Scap* fail to engage in blastogenesis and proliferation induced by the T cell antigen receptor and exhibit decreased glycolysis and OxPhos¹⁴. The decreases in growth and proliferation are partially 'rescued' by supplementing the T cells with cholesterol, which indicates that the diminished cholesterol synthesis in *Scap*^{KO} T cells contributes to this phenotype¹⁴. However, it remains to be determined whether *Scap*^{KO} CD8⁺ T cells have diminished glycolysis and OxPhos due to a failure to induce the citrate–malate shuttle. Srebp transcription factors have also been described as having immunoregulatory roles in CD4⁺ T cells that are independent of cellular metabolism. In T_H17 cells, Srebp has been proposed to have a direct role in controlling the expression of *Il17* (ref. 32). Srebp also controls macrophage function through regulation of inflammasome and interferon signaling dependent on the membrane-associated adaptor STING^{33–35}. Therefore, Srebp and Srebp-controlled metabolic processes are emerging as being important in the regulation of immune responses.

Here we described a previously unknown metabolic configuration for activated lymphocytes: cytokine-stimulated NK cells reprogrammed their cellular metabolic pathways to maintain elevated levels of glycolysis and OxPhos through the use of the citrate–malate shuttle. *Acy* and *Slc25a1*, which encode the key components of that shuttle, are both described as Srebp1 targets, and indeed it was expression of the Srebp1c isoform that was robustly induced in cytokine-stimulated NK cells^{16,25–29}. The citrate–malate shuttle allows glycolysis-derived NADH to be converted into mitochondrial NADH

to fuel OxPhos and ATP synthesis. It is more commonly accepted that the malate–aspartate shuttle is responsible for this function, but this is not the case in NK cells. The malate–aspartate shuttle only transports electrons into the mitochondria whereas, the citrate–malate shuttle also exports acetyl-CoA from the mitochondria into the cytosol, via citrate. While this metabolic circuit has not been studied directly in other immune cells, various subsets of immune cells, including memory T cells and M2 macrophages, have been reported to metabolize glucose into cytosolic acetyl-CoA, which indicates that the citrate–malate shuttle is probably also important in these cells^{36,37}. In NK cells, providing acetyl-CoA for lipid synthesis is not important for their growth, proliferation or effector function, which raises the question of why the citrate–malate shuttle is used in these cells. One possibility is that NK cells adopt this particular metabolic circuit because it supplies acetyl-CoA for acetylation reactions. Histone acetylation has been shown to be important in NK cells in the regulation of multiple genes that encode receptors and effector molecules, including the activating receptor NKG2D and IFN- γ ^{38–40}. In monocytes, the metabolic changes that occur following activation are crucial for trained innate immunity, an epigenetic process that leads to enhanced responsiveness to secondary infections⁴¹. Indeed, NK cells have been reported to have some forms of innate immunological memory, and epigenetic changes are important in this process^{42–44}. The NK cell metabolic phenotype described here might provide a mechanism for the regulation of such NK cell memory responses.

While the relationships among Srebp signaling, the citrate–malate shuttle and rates of OxPhos are relatively straightforward, the reasons for the importance of Srebp and the citrate–malate shuttle in elevated glycolysis are less obvious. When the citrate–malate shuttle was inhibited, the glycolytic capacity decreased; this would suggest that the citrate–malate shuttle is an important source of cytosolic NAD⁺, which is needed to sustain GAPDH activity and, by extension, elevated glycolytic rates. The citrate–malate shuttle might also affect maximum glycolytic rates by providing acetyl-CoA for the acetylation of GAPDH, as it has been shown that the acetylation of GAPDH in CD8⁺ T cells enhances its catalytic activity⁴⁵.

The activation of Srebp transcription factors involves the translocation of Srebp from the endoplasmic reticulum to the Golgi, which is inhibited by both cholesterol and the oxysterol 25HC¹⁸. It will be of interest to determine whether the activation of Srebp and NK cell metabolism are compromised in patients with elevated levels of cholesterol or oxysterols^{46,47}. Also, it is worth noting that cancer cells have been reported to produce and secrete oxysterols, including 25HC, although so far the effect of these molecules on the anti-tumor immune response has not been considered in detail^{48,49}. Additionally, interferon-stimulated macrophages have high expression of cholesterol 25-hydroxylase, the enzyme that oxidizes cholesterol to generate 25HC, and macrophage-derived 25HC is emerging as being important in the regulation of inflammatory responses^{35,50}. Therefore, the finding that NK cells required Srebp activity for their metabolic and functional responses has revealed a previously unknown mechanism for the regulation of NK cell responses by cholesterol and 25HC. Future work should focus on investigating whether the dysfunctional NK cell phenotypes observed in various pathological settings might be due, at least in part, to defective Srebp activity and failed NK cell metabolism.

METHODS

Methods, including statements of data availability and any associated accession codes and references, are available in the [online version of the paper](#).

Note: Any Supplementary Information and Source Data files are available in the online version of the paper.

ACKNOWLEDGMENTS

We thank the Comparative Medicine Unit, Trinity College Dublin for use of their facilities. Supported by Science Foundation Ireland (12/IP/1286 and 13/CDA/2161 for the D.K.F. laboratory); Irish Cancer Society (research scholarship CRS15OBR to K.L.O'B. which includes support from the Children's Leukaemia Research Project), Coordenadoria de Aperfeiçoamento de Pessoal de Nível Superior (CAPES), Brazil (research scholarship BEX 13446134 to V.Z.B.) and Deutsche Forschungsgemeinschaft (KFO-262 for K.D.).

AUTHOR CONTRIBUTIONS

Conceptualization, N.A., R.P.D. and D.K.F.; methodology, N.A., R.P.D., L.D., V.Z.-B., C.M.G., K.D. and D.K.F.; investigation, N.A., K.L.O'B. R.P.D., L.D., V.Z.-B., R.M.L., K.D. and P.H.; writing (original draft), N.A. and D.K.F.; writing (review and editing), N.A., K.L.O'B., P.J.O., C.M.G. and D.K.F.; and supervision, P.J.O., L.L., C.M.G. and D.K.F.

COMPETING FINANCIAL INTERESTS

The authors declare no competing financial interests.

Reprints and permissions information is available online at <http://www.nature.com/reprints/index.html>. Publisher's note: Springer Nature remains neutral with regard to jurisdictional claims in published maps and institutional affiliations.

- Pearce, E.L., Poffenberger, M.C., Chang, C.H. & Jones, R.G. Fueling immunity: insights into metabolism and lymphocyte function. *Science* **342**, 1242454 (2013).
- Loftus, R.M. & Finlay, D.K. Immunometabolism: cellular metabolism turns immune regulator. *J. Biol. Chem.* **291**, 1–10 (2016).
- Assmann, N. & Finlay, D.K. Metabolic regulation of immune responses: therapeutic opportunities. *J. Clin. Invest.* **126**, 2031–2039 (2016).
- Caligiuri, M.A. Human natural killer cells. *Blood* **112**, 461–469 (2008).
- Lynch, L.A. *et al.* Are natural killer cells protecting the metabolically healthy obese patient? *Obesity* **17**, 601–605 (2009).
- O'Shea, D., Cawood, T.J., O'Farrelly, C. & Lynch, L. Natural killer cells in obesity: impaired function and increased susceptibility to the effects of cigarette smoke. *PLoS One* **5**, e8660 (2010).
- Laue, T. *et al.* Altered NK cell function in obese healthy humans. *BMC Obes.* **2**, 1 (2015).
- Gardiner, C.M. NK cell function and receptor diversity in the context of HCV infection. *Front. Microbiol.* **6**, 1061 (2015).
- Oliviero, B. *et al.* Natural killer cell functional dichotomy in chronic hepatitis B and chronic hepatitis C virus infections. *Gastroenterology* **137**, 1151–1160 (2009).
- Arnold, M. *et al.* Global burden of cancer attributable to high body-mass index in 2012: a population-based study. *Lancet Oncol.* **16**, 36–46 (2015).
- Sun, Y. *et al.* Weight and prognosis for influenza A(H1N1)pdm09 infection during the pandemic period between 2009 and 2011: a systematic review of observational studies with meta-analysis. *Infect. Dis.* **48**, 813–822 (2016).
- Donnelly, R.P. *et al.* mTORC1-dependent metabolic reprogramming is a prerequisite for NK cell effector function. *J. Immunol.* **193**, 4477–4484 (2014).
- Keating, S.E. *et al.* Metabolic reprogramming supports IFN- γ production by CD56^{bright} NK cells. *J. Immunol.* **196**, 2552–2560 (2016).
- Kidani, Y. *et al.* Sterol regulatory element-binding proteins are essential for the metabolic programming of effector T cells and adaptive immunity. *Nat. Immunol.* **14**, 489–499 (2013).
- Berod, L. *et al.* De novo fatty acid synthesis controls the fate between regulatory T and T helper 17 cells. *Nat. Med.* **20**, 1327–1333 (2014).
- Shimomura, I., Shimano, H., Korn, B.S., Bashmakov, Y. & Horton, J.D. Nuclear sterol regulatory element-binding proteins activate genes responsible for the entire program of unsaturated fatty acid biosynthesis in transgenic mouse liver. *J. Biol. Chem.* **273**, 35299–35306 (1998).
- Düvel, K. *et al.* Activation of a metabolic gene regulatory network downstream of mTOR complex 1. *Mol. Cell* **39**, 171–183 (2010).
- Horton, J.D., Goldstein, J.L. & Brown, M.S. SREBPs: activators of the complete program of cholesterol and fatty acid synthesis in the liver. *J. Clin. Invest.* **109**, 1125–1131 (2002).
- Radhakrishnan, A., Ikeda, Y., Kwon, H.J., Brown, M.S. & Goldstein, J.L. Sterol-regulated transport of SREBPs from endoplasmic reticulum to Golgi: oxysterols block transport by binding to Insig. *Proc. Natl. Acad. Sci. USA* **104**, 6511–6518 (2007).
- Hawkins, J.L. *et al.* Pharmacologic inhibition of site 1 protease activity inhibits sterol regulatory element-binding protein processing and reduces lipogenic enzyme gene expression and lipid synthesis in cultured cells and experimental animals. *J. Pharmacol. Exp. Ther.* **326**, 801–808 (2008).
- Bakan, I. & Laplante, M. Connecting mTORC1 signaling to SREBP-1 activation. *Curr. Opin. Lipidol.* **23**, 226–234 (2012).
- Hameyer, D. *et al.* Toxicity of ligand-dependent Cre recombinases and generation of a conditional Cre deleter mouse allowing mosaic recombination in peripheral tissues. *Physiol. Genomics* **31**, 32–41 (2007).
- Sun, T., Hayakawa, K., Bateman, K.S. & Fraser, M.E. Identification of the citrate-binding site of human ATP-citrate lyase using X-ray crystallography. *J. Biol. Chem.* **285**, 27418–27428 (2010).
- Gnoni, G.V., Priore, P., Geelen, M.J. & Siculella, L. The mitochondrial citrate carrier: metabolic role and regulation of its activity and expression. *IUBMB Life* **61**, 987–994 (2009).
- Sato, R. *et al.* Transcriptional regulation of the ATP citrate-lyase gene by sterol regulatory element-binding proteins. *J. Biol. Chem.* **275**, 12497–12502 (2000).
- Shimano, H. *et al.* Sterol regulatory element-binding protein-1 as a key transcription factor for nutritional induction of lipogenic enzyme genes. *J. Biol. Chem.* **274**, 35832–35839 (1999).
- Amemiya-Kudo, M. *et al.* Transcriptional activities of nuclear SREBP-1a, -1c, and -2 to different target promoters of lipogenic and cholesterologenic genes. *J. Lipid Res.* **43**, 1220–1235 (2002).
- Moon, Y.A., Lee, J.J., Park, S.W., Ahn, Y.H. & Kim, K.S. The roles of sterol regulatory element-binding proteins in the transactivation of the rat ATP citrate-lyase promoter. *J. Biol. Chem.* **275**, 30280–30286 (2000).
- Infantino, V., Iacobazzi, V., De Santis, F., Mastrapasqua, M. & Palmieri, F. Transcription of the mitochondrial citrate carrier gene: role of SREBP-1, upregulation by insulin and downregulation by PUFA. *Biochem. Biophys. Res. Commun.* **356**, 249–254 (2007).
- Guillerey, C., Huntington, N.D. & Smyth, M.J. Targeting natural killer cells in cancer immunotherapy. *Nat. Immunol.* **17**, 1025–1036 (2016).
- Ni, J., Miller, M., Stojanovic, A., Garbi, N. & Cerwenka, A. Sustained effector function of IL-12/15/18-primed NK cells against established tumors. *J. Exp. Med.* **209**, 2351–2365 (2012).
- Cui, G. *et al.* Liver X receptor (LXR) mediates negative regulation of mouse and human Th17 differentiation. *J. Clin. Invest.* **121**, 658–670 (2011).
- York, A.G. *et al.* Limiting cholesterol biosynthetic flux spontaneously engages type I IFN signaling. *Cell* **163**, 1716–1729 (2015).
- Im, S.S. *et al.* Linking lipid metabolism to the innate immune response in macrophages through sterol regulatory element binding protein-1a. *Cell Metab.* **13**, 540–549 (2011).
- Reboldi, A. *et al.* Inflammation. 25-Hydroxycholesterol suppresses interleukin-1-driven inflammation downstream of type I interferon. *Science* **345**, 679–684 (2014).
- O'Sullivan, D. *et al.* Memory CD8⁺ T cells use cell-intrinsic lipolysis to support the metabolic programming necessary for development. *Immunity* **41**, 75–88 (2014).
- Huang, S.C. *et al.* Cell-intrinsic lysosomal lipolysis is essential for alternative activation of macrophages. *Nat. Immunol.* **15**, 846–855 (2014).
- Fernández-Sánchez, A. *et al.* DNA demethylation and histone H3K9 acetylation determine the active transcription of the NKG2D gene in human CD8⁺ T and NK cells. *Epigenetics* **8**, 66–78 (2013).
- Chang, S. & Aune, T.M. Histone hyperacetylated domains across the *lfn3* gene region in natural killer cells and T cells. *Proc. Natl. Acad. Sci. USA* **102**, 17095–17100 (2005).
- Miyake, T. *et al.* I κ B ζ is essential for natural killer cell activation in response to IL-12 and IL-18. *Proc. Natl. Acad. Sci. USA* **107**, 17680–17685 (2010).
- Cheng, S.C. *et al.* mTOR- and HIF-1 α -mediated aerobic glycolysis as metabolic basis for trained immunity. *Science* **345**, 1250684 (2014).
- Cerwenka, A. & Lanier, L.L. Natural killer cell memory in infection, inflammation and cancer. *Nat. Rev. Immunol.* **16**, 112–123 (2016).
- Cooper, M.A. *et al.* Cytokine-induced memory-like natural killer cells. *Proc. Natl. Acad. Sci. USA* **106**, 1915–1919 (2009).
- Romee, R. *et al.* Cytokine activation induces human memory-like NK cells. *Blood* **120**, 4751–4760 (2012).
- Balmer, M.L. *et al.* Memory CD8⁺ T Cells require increased concentrations of acetate induced by stress for optimal function. *Immunity* **44**, 1312–1324 (2016).
- Murakami, H., Tamasawa, N., Matsui, J., Yasujima, M. & Suda, T. Plasma oxysterols and tocopherol in patients with diabetes mellitus and hyperlipidemia. *Lipids* **35**, 333–338 (2000).
- Bertolotti, M. *et al.* Increased appearance rate of 27-hydroxycholesterol in vivo in hypercholesterolemia: a possible compensatory mechanism. *Nutr. Metab. Cardiovasc. Dis.* **22**, 823–830 (2012).
- Eibinger, G. *et al.* On the role of 25-hydroxycholesterol synthesis by glioblastoma cell lines. Implications for chemotactic monocyte recruitment. *Exp. Cell Res.* **319**, 1828–1838 (2013).
- York, A.G. & Bensinger, S.J. Subverting sterols: rerouting an oxysterol-signaling pathway to promote tumor growth. *J. Exp. Med.* **210**, 1653–1656 (2013).
- Gold, E.S. *et al.* 25-Hydroxycholesterol acts as an amplifier of inflammatory signaling. *Proc. Natl. Acad. Sci. USA* **111**, 10666–10671 (2014).

ONLINE METHODS

Mice. C57BL/6J mice were purchased from Harlan or Charles River or were bred in house. *Scap*-floxed mice (B6;129-*Scap*^{tm1Mbjg/J})⁵¹ were obtained from the Jackson Laboratory. Tamox-Cre mice (Gt(ROSA)26Sortm2(cre/ERT2)Brn/Cnrn)²² were obtained from the EMMA archive. All mice were and maintained in compliance with EU and the Health Products Regulatory Authority regulations with the approval of the University of Dublin's ethical review board.

Cell culture. Cells were cultured in RPMI medium (Invitrogen/Biosciences) supplemented with 2 mM L-glutamine (Invitrogen/Biosciences), 10% heat-inactivated FCS (Labtech International), 50 μ M β -mercaptoethanol (Sigma) and 1% penicillin-streptomycin (Invitrogen/Biosciences). For NK cell culture, splenocytes were isolated from mouse spleen and were cultured in IL-15 (10 ng/ml, Peprotech; in RPMI medium) as described previously¹². On day 6, cells were stimulated with the cytokine combinations IL-2 (20 ng/ml, NCI preclinical repository) plus IL-12 (10 ng/ml, Miltenyi Biotech), or IL-12 (25 ng/ml) plus IL-15 (50 ng/ml, Peprotech) plus IL-18 (5 ng/ml, R&D Systems). Unstimulated cells were maintained in a low dose of IL-15 (5 ng/ml) as a survival factor. The cells were stimulated in the presence or absence of the inhibitors 25-hydroxycholesterol (25HC, 0.83–5 μ M Sigma), PF429242 (10 μ M, Adoog Bioscience), BMS303141 (10 μ M for Seahorse analysis and 50 μ M for flow cytometry analysis, Sigma), SB204990 (30 μ M, Tocris), C75 (39.3 μ M, Cambridge Biosciences), 5-(tetradecyloxy)-2-furoic acid (TOFA, 15.4 μ M, Cambridge Biosciences) or rapamycin (20 nM, Fisher). For biochemical analyses, NK cells were purified from culture after day 6, by magnetic-activated cell sorting (MACS) using the NK cell isolation kit II (Miltenyi Biotech). Where indicated, splenocytes were isolated from *Scap*^{KO} (*Scap*^{fl/fl} \times Tamox-Cre) mice or *Scap*^{WT} (*Scap*^{+/+} \times Tamox-Cre) mice. Splenocytes were cultured for 3 d in IL-15 (10 ng/ml, Peprotech; in RPMI medium) in the presence of 4-hydroxytamoxifen (0.6 μ M, Sigma) to induce Cre recombinase-mediated excision of the floxed *Scap* exon. For T cell culture, splenocytes were isolated from mouse spleen and T cells were activated with antibody to CD3 (anti-CD3) (2c11, 500 ng/ml) and IL-2 (20 ng/ml, NCI preclinical repository) in RPMI medium for 36 h at 10×10^6 cells/ml. Following activation, cells were washed and maintained in IL-2 (20 ng/ml). Cells were re-fed IL-2 (20 ng/ml), and the cell concentration was adjusted to 0.3×10^6 cells/ml every 24 h for a further 5 d. For analysis of cytotoxicity YAC-1 cells (mouse lymphoma cell line) and K562 cells (human chronic myelogenous leukemia cell line) were cultured in either RPMI 1640 (Invitrogen/Biosciences) or Iscove's modified Dulbecco's medium (Sigma), both supplemented with 2 mM L-glutamine (Invitrogen, Biosciences), 10% heat-inactivated FCS (Labtech, International) and 1% penicillin-streptomycin (Invitrogen/Biosciences). B16-F10 mouse melanoma cells were cultured in DMEM medium supplemented with 10% heat-inactivated FCS and 1% penicillin-streptomycin. YAC-1, K562 and B16-F10 cell lines were purchased from the American Type Culture Collection.

Human NK cell isolation and cell culture. Blood samples were obtained from healthy donors from whom written consent had been obtained. Ethics was granted by the local Trinity College Dublin research ethics committee. Peripheral blood mononuclear cells were isolated by Lymphoprep gradient (Axis-Shield). 5×10^6 peripheral blood mononuclear cells per ml were incubated at 37 °C for 18 h in RPMI 1640 GlutaMAX medium (Life Technologies, Invitrogen) supplemented with 10% heat-inactivated FCS (Labtech International) and 1% penicillin-streptomycin (Invitrogen, Biosciences) and were stimulated with IL-12 (30 ng/ml, Miltenyi Biotech) and IL-15 (100 ng/ml, NCI preclinical repository). Where indicated, cells were cultured with or without the inhibitors PF429242 (10 μ M), 25HC (5 μ M) or BMS303141 (50 μ M).

T cell proliferation. Cultured T cells were cultured at 0.3×10^6 cell/ml in IL-2 (20 ng/ml) in the presence or absence of 25HC (2.5 μ M), PF429242 (10 μ M) or TOFA (15.4 μ M). Proliferation was assessed by cell counts after 48 h. No significant differences in cell survival were observed, as determined by flow cytometry.

Flow cytometry. Cells were incubated for 10 min at 4 °C with Fc blocking antibody CD16/CD32 (2.4G2) and were subsequently stained for 20 min at 4 °C with saturating concentrations of antibodies. Antibodies used were as follows: NK1.1-eFluor 450 (PK136), NKp46-PerCPeFluor 710 (29A1.4), NKp46-PE (29A1.4), CD3-FITC (145-2C11) and granzyme B-PE-Cy7 (NGZB), all purchased from eBiosciences; TCR β -APC (H57-597), CD69-PerCp-Cy5.5 (H1.2F3), CD25-APC-Cy7 (PC61), CD71-PE (C2), IFN- γ -APC (XMG1.2), CD19-PE-Cy7 (1D3), CD8a-PerCp-Cy5.5 (53-6.7) and CD4-PE-Cy7 (RM4-5), all purchased from BD Biosciences; and NK1.1-BV421 (PK136), from BioLegend. Live cells were gated according to their forward scatter (FSC-A) and side scatter (SSC-A); single cells were gated according to their FSC-W and FSC-A; and NK cells were identified as NK1.1⁺NKp46⁺CD3⁻ cells. For intracellular staining, the cells were incubated for 4 h with the protein-transport inhibitor GolgiPlug (BD Biosciences). For fixation and permeabilization of the cells, the Cytofix/Cytoperm kit from BD Biosciences was used according to the manufacturer's instruction. For proliferation studies, NK cells were stained on day 3 of culture with the CellTrace CFSE kit (Molecular Probes) according to the manufacturer's instruction. Cells were cultured for 2 d in medium containing IL-2 (20 ng/ml) and IL-12 (10 ng/ml) in the presence or absence of the inhibitors PF429242 (10 μ M), 25HC (0.83 μ M), TOFA (15.4 μ M) and C75 (39.3 μ M) and were analyzed every day by dilution of the dye CFSE. For mitochondrial mass experiments, cells were incubated in medium containing MitoTracker Red CMXRos (100 nM, ThermoFisher) for 30 min at 37 °C, before further staining and analysis. For analysis of human NK cells, antibodies to the following were used: CD56 (HCD56/NCAM16.2), CD3 (SK7/UCHT1) granzyme B (GB11) and IFN- γ (B27), purchased from BD Pharmingen. Data were acquired on a FACSCanto, a LSR Fortessa or a FACSCalibur (Becton Dickinson) and were analyzed using FlowJo software (TreeStar).

Quantitative real-time PCR. Cultured NK cells were purified by MACS with the NK isolation kit II (Miltenyi Biotech) before stimulation. RNA was isolated using the RNeasy RNA purification mini kit (QIAGEN) according to the manufacturer's protocol. From purified RNA, cDNA was synthesized using the reverse-transcriptase kit qScript cDNA synthesis kit (Quanta Biosciences). Quantitative real-time PCR (qRT-PCR) was performed in triplicate in a 96-well plate using iQ SYBR Green-based detection on an ABI 7900HT Fast qRT-PCR machine. For the analysis of mRNA abundance, the derived values were normalized to those of *Rplp0* or *Gapdh* mRNA. Primer sequences are in **Supplementary Table 1**.

Lipid synthesis. Cultured NK cells were washed with FCS-free medium and resuspended in FCS-free medium containing lipoprotein-deficient serum (LPDS, Enzo Life Sciences) at a concentration of 4×10^6 cells per ml, and ¹⁴C₂-acetate (85 μ M final concentration, PerkinElmer) added. The cells were incubated for 4 h and were washed twice with PBS before lysis with 0.5% Triton X-100. Lipids were extracted by methanol-chloroform-water extraction (2/2/1, v/v/v) and were transferred into scintillation vials. The organic solvent was allowed to evaporate completely, and the lipids were dissolved in 3 ml of Ultima Gold LSC cocktail (Sigma-Aldrich) and analyzed using a scintillation counter. The resulting disintegrations per minute (dpm) values were converted to nmol of acetate incorporated per 10^6 cells.

Seahorse metabolic flux analyzer. For real-time analysis of the extracellular acidification rate (ECAR) and oxygen-consumption rate (OCR) of purified NK cells cultured under various conditions or CTLs, a Seahorse XF-24 Analyzer (Seahorse Bioscience) was used. In brief, 5×10^5 to 7.5×10^5 NK cells or CTLs purified by MACS were made to adhere to a 24-well XF Cell Culture Microplate (Seahorse Biosciences) coated with Cell-Tak™ (Corning). Sequential measurements of ECAR and OCR made after the addition of the inhibitors (Sigma) oligomycin (2 μ M), FCCP (0.5 μ M), rotenone (100 nM) plus antimycin A (4 μ M), and 2-deoxyglucose (2DG, 30 mM) allowed calculation of basal glycolysis, glycolytic capacity, basal mitochondrial respiration and maximal mitochondrial respiration (**Supplementary Fig. 3**). Where indicated, BMS303141 (10 μ M, Sigma), SB204990 (30 μ M, Tocris), dimethyl malonate (10 mM, Sigma) and aminooxyacetic acid (0.5 mM, Viva Bioscience LTD) were injected into the Seahorse plate. An equivalent amount of vehicle

was injected into control wells. ECAR and OCR measurements were normalized to those of 1×10^6 NK or CTL cells.

Stable isotope tracer analysis. For analysis of TCA-cycle intermediates, 4×10^6 purified cultured NK cells were stimulated for 18 h in medium containing either 10 mM unlabeled glucose or 10 mM $^{13}\text{C}_6$ -glucose (purity 98.4%, CK Isotopes Limited), in the presence or absence of 25HC. Label incorporation from uniformly labeled $^{13}\text{C}_6$ -glucose into fatty acids and amino acids were analyzed. For time course experiments, purified cultured NK cells were stimulated for 16 h in medium containing IL-2 (20 ng/ml) plus IL-12 (10 ng/ml). The cells were washed three times in medium without glucose, then 4×10^6 NK cells were cultured for another 30 min to 8 h in medium containing IL-2 (20 ng/ml) plus IL-12 (10 ng/ml) and 10 mM $^{13}\text{C}_6$ -glucose (purity 98.4%, CK Isotopes Limited). For all experiments, cells were harvested and washed three times with ice-cold PBS. TCA-cycle intermediates and amino acids metabolites were extracted from the cell pellet and cell culture supernatant by adding 80% aqueous methanol. Lipids were extracted from the cell pellet using chloroform. Extracts were dried using a centrifugal evaporator (GeneVac EZ-2, SP Scientific) and were stored at -80°C until further processing. Cell pellets from the experiment with unlabeled glucose were spiked with 10 μl internal standard solution containing [^{13}C] fumarate, succinate-d4 and citrate-d4 at 1 mM each. Calibration curves for each analyte with the corresponding stable isotope labeled analog as internal standard were used to obtain quantitative data.

For the analysis of lactate through glycolysis or the PPP, cells were stimulated in medium containing 1,2- $^{13}\text{C}_2$ -glucose (purity 99.7%, CK Isotopes Limited). After stimulation, 1 ml of cell culture stimulation medium was centrifuged at 2,000g and 4°C for 5 min, and the supernatant was transferred to a new Eppendorf tube and stored at -80°C until further processing.

For stable isotope tracer experiments, the analysis accounted for all isotopologues of a specific metabolite.

Liquid chromatography–tandem mass spectrometry. Unlabeled metabolites of the TCA cycle and isotopologues of succinate, fumarate and citrate were analyzed by HPLC-ESI-MS/MS using an API 4000 QTrap mass spectrometer (ABSciex) coupled to a 1200 SL HPLC system (Agilent). Negative-mode ionization and multiple reaction monitoring (MRM) were employed for detection. Separation was carried out on a Discovery HS F5-3 HPLC column (150 mm \times 2.1 mm, 3 μm ; Supelco) with a Security Guard column (C18, Phenomenex) and gradient elution with 0.1% formic acid in water (v/v) as mobile phase A and acetonitrile as mobile phase B. MRM transitions for each isotopologue were monitored. For isotopologue analysis of amino acids, a 10- μl aliquot of the cellular extract was subjected to derivatization with propyl chloroformate–propanol and HPLC-ESI-MS/MS analysis as previously described⁵². MRM transitions for each isotopologue were monitored.

GC-MS analysis. To determine extracellular lactate, 10 μl supernatant was dried (CombiDancer Hettich AG) and subjected to methoximation and silylation employing the derivatization protocol and instrumental setup previously described⁵³. 1 μl of the derivatized sample was injected using split mode with a split ratio of 8:1. To analyze intracellular TCA-cycle intermediates, cell extracts were dried and subjected to derivatization and GC analysis as described above with the exception that splitless injection was performed.

Fatty-acid analysis was performed after trans-methylation via adaptation of a published protocol⁵⁴. The chloroform extract was spiked with 10 μl internal standard containing odd-numbered, saturated straight chain fatty acids (C9–C19) at a concentration of 1 mM and the solvent was evaporated. Then, 100 μl butylated hydroxytoluene (0.5 mg/ml in methanol) was added to the residue, followed by 1,500 μl derivatization reagent consisting of 83 μl acetyl chloride in 1,417 μl methanol. The mixture was incubated at 100°C for 1 h, and methyl esters were then extracted twice with 750 μl hexane. The extracts were combined and evaporated to dryness. The residue was reconstituted in 60 μl hexane before GC-MS analysis. Fatty-acid methyl-ester analysis was performed using a SLB-IL82 column (30 m \times 0.25 mm I.D., 0.2- μm film thickness, Supelco) with a 1 m guard column and the instrumental equipment previously described⁵⁵. The initial oven temperature was set at 50°C (1 min) and was ramped at 5°C per min to a final temperature of 265°C (10 min). The carrier gas was helium with a flow rate of 0.7 ml/min. Injection was performed in splitless

mode at 270°C using an injection volume of 1 μl . The mass spectrometer was operated in full-scan mode from 60 m/z to 500 m/z.

Data analysis for MS and MS/MS data. Lactate isotopologues were determined using the fragment ions 192 and 193 for $^{13}\text{C}_1$ - and $^{13}\text{C}_2$ -labeled lactate, respectively. For analysis of the LC-MS/MS data, the software Analyst (version 1.6.2) was used. GC-MS data was analyzed using the software Mass Hunter (version B.07.01/Build 7.1.524.0). All raw data were corrected for natural abundance and tracer impurity using the software IsoCor (Software Version 1.0)⁵⁶ for the GC-MS data, and an in-house tool was used to correct MS/MS data. For comparison of the label incorporation of several metabolites, the mean isotopic enrichment (ME) is presented. For this calculation, the following formula was used:

$$ME = \frac{\sum_{i=0}^n M_i \times i}{n}$$

with n as the number of tracer atoms in the metabolite and M_i as the relative proportion of the metabolite with i tracer atoms⁵⁶. The abundance of each metabolite was normalized to that of 1×10^6 cells.

Immunoblot analysis. For immunoblot analysis, cells were harvested, washed twice with ice-cold PBS and lysed at 1×10^7 cells per ml in lysis buffer containing 50 mM Tris-HCl pH 6.7, 2% SDS, 10% glycerol, 0.05% bromophenol blue, 1 μM DTT, phosphatase and protease inhibitors. Samples were boiled at 95°C for 10 min, separated by SDS-PAGE and transferred to a PVDF membrane. Blots were probed with antibody to ribosomal protein S6 phosphorylated at Ser235 and Ser236 (#2211), antibody to S6K phosphorylated at T389 (#9234) and anti-PKB (#9272) (all from Cell Signaling Technologies), and anti- β -actin (A5441) (Sigma-Aldrich).

Cytotoxicity assay. For the measurement of NK cell cytotoxicity, NK cells were stimulated for 18 h in medium containing IL-2 (20 ng/ml) plus IL-12 (10 ng/ml) or in IL-12 (25 ng/ml) plus IL-15 (50 ng/ml) plus IL-18 (5 ng/ml), with or without the inhibitors 25HC (2.5 μM), PF429242 (10 μM) or TOFA (15.4 μM). YAC-1 or K652 target cells were stained with 10 μM calcein-AM (BD Pharmingen) at 37°C for 30 min. 2×10^4 to 3×10^4 stained target cells were added to a 96-well V-bottomed plate, and NK cells were added in a NK cell/target cell ratio of 5:1, 2:1 or 1:1. For measurement of spontaneous release and maximum release, only target cells were added to the well or a final concentration of 0.2% Triton X-100 lysis buffer was added to target cells, respectively. Cells were incubated for 4 h at 37°C . After incubation, the plate was spun down at 200g for 5 min, and 75 μl supernatant was transferred to a black 96-well plate. Fluorescence was measured on a Molecular Probes Spectra Max M3 spectrometer with an excitation wavelength of 495 nm and an emission wavelength of 515 nm. All samples were measured in triplicate, and the average was used for further analysis.

B16 tumor model. B16 cells were used for tumor induction in C57BL/6 mice, by subcutaneous injection of 2×10^5 cells per mouse into the right flank. On days 3, 7 and 10 after tumor induction, mice were given subcutaneous injection, into the tumor site, of PBS or NK cells (1.2×10^6 to 2×10^6 cells per mouse) stimulated *in vitro* for 18 h with IL-12 (25 ng/ml) plus IL-15 (50 ng/ml) plus IL-18 (5 ng/ml) with or without 25HC (2.5 μM). Tumor growth was recorded every 2–3 d, and mice were killed when tumors reached a size of 15 mm in diameter (D) or on day 15. Tumor size was calculated using the following formula: $(D1)^2 \times (D2/2)$, with D1 being the smaller value of the tumor diameter.

Statistical analysis. GraphPad Prism 6.00 (GraphPad Software) was used for statistical analysis. A one-way ANOVA test was used for the comparison of more than two groups throughout, with the Tukey or Sidak test for multiple comparisons. Analysis of data with two factors were analyzed by a two-way ANOVA with the Sidak test for multiple comparison. A two-tailed Student's t -test was used when there were only two groups for analysis. For comparison of relative values, a one-sample t -test was used to calculate P values with the theoretical value set as 1.00 or 0.00. For human data, a Wilcoxon test was used to compare two groups, and a one-way ANOVA with a Holm-Sidak test for multiple comparison was used for the analysis of more than two groups. A P value

of ≤ 0.05 was considered statistically significant. In all figures, $*P \leq 0.05$, $**P \leq 0.01$, $***P \leq 0.001$ and $****P \leq 0.0001$.

A **Life Sciences Reporting Summary** for this paper is available.

Data availability. The data that support the findings of this study are available from the corresponding author upon request. The in-house tool for the correction of natural abundance of MS/MS data is available upon request.

51. Matsuda, M. *et al.* SREBP cleavage-activating protein (SCAP) is required for increased lipid synthesis in liver induced by cholesterol deprivation and insulin elevation. *Genes Dev.* **15**, 1206–1216 (2001).

52. van der Goot, A.T. *et al.* Delaying aging and the aging-associated decline in protein homeostasis by inhibition of tryptophan degradation. *Proc. Natl. Acad. Sci. USA* **109**, 14912–14917 (2012).

53. Dettmer, K. *et al.* Metabolite extraction from adherently growing mammalian cells for metabolomics studies: optimization of harvesting and extraction protocols. *Anal. Bioanal. Chem.* **399**, 1127–1139 (2011).

54. Masood, A., Stark, K.D. & Salem, N. Jr. A simplified and efficient method for the analysis of fatty acid methyl esters suitable for large clinical studies. *J. Lipid Res.* **46**, 2299–2305 (2005).

55. Dettmer, K. Assessment of ionic liquid stationary phases for the GC analysis of fatty acid methyl esters. *Anal. Bioanal. Chem.* **406**, 4931–4939 (2014).

56. Millard, P., Letisse, F., Sokol, S. & Portais, J.C. IsoCor: correcting MS data in isotope labeling experiments. *Bioinformatics* **28**, 1294–1296 (2012).

Life Sciences Reporting Summary

Nature Research wishes to improve the reproducibility of the work that we publish. This form is intended for publication with all accepted life science papers and provides structure for consistency and transparency in reporting. Every life science submission will use this form; some list items might not apply to an individual manuscript, but all fields must be completed for clarity.

For further information on the points included in this form, see [Reporting Life Sciences Research](#). For further information on Nature Research policies, including our [data availability policy](#), see [Authors & Referees](#) and the [Editorial Policy Checklist](#).

▶ Experimental design

1. Sample size

Describe how sample size was determined.

Based on extensive experience in biochemical analysis 3-5 replicates provide adequate statistical power.
For the in vivo tumour experiments a sample size of 15 was calculated using a power analysis with a data set generated by colleague within TCD that uses this model regularly.

2. Data exclusions

Describe any data exclusions.

For all biochemical analysis parallel flow cytometry analysis was performed to look at establish patterns of NK cell activation in terms of cell size, activation marker expression, IFN γ production and granzyme b expression. When normal patterns of NK cell activation were not observed, data from biochemical analyses were excluded.

For seahorse analysis, we did parallel viability analyses. Experiments were excluded if significant difference in viability were observed between the different experimental conditions.

3. Replication

Describe whether the experimental findings were reliably reproduced.

All attempts of replication were successful.

4. Randomization

Describe how samples/organisms/participants were allocated into experimental groups.

NA

5. Blinding

Describe whether the investigators were blinded to group allocation during data collection and/or analysis.

NA

Note: all studies involving animals and/or human research participants must disclose whether blinding and randomization were used.

6. Statistical parameters

For all figures and tables that use statistical methods, confirm that the following items are present in relevant figure legends (or in the Methods section if additional space is needed).

- n/a Confirmed
- The exact sample size (n) for each experimental group/condition, given as a discrete number and unit of measurement (animals, litters, cultures, etc.)
 - A description of how samples were collected, noting whether measurements were taken from distinct samples or whether the same sample was measured repeatedly
 - A statement indicating how many times each experiment was replicated
 - The statistical test(s) used and whether they are one- or two-sided (note: only common tests should be described solely by name; more complex techniques should be described in the Methods section)
 - A description of any assumptions or corrections, such as an adjustment for multiple comparisons
 - The test results (e.g. P values) given as exact values whenever possible and with confidence intervals noted
 - A clear description of statistics including central tendency (e.g. median, mean) and variation (e.g. standard deviation, interquartile range)
 - Clearly defined error bars

See the web collection on [statistics for biologists](#) for further resources and guidance.

► Software

Policy information about [availability of computer code](#)

7. Software

Describe the software used to analyze the data in this study.

Software used was FlowJo 8 and 10, Mass Hunter (version B.07.01/Build 7.1.524.0), Analyst (version 1.6.2), IsoCor (Software Version 1), in-house tool for correction of MS/MS data for natural abundance, GraphPad Prism 6, Excel, ImageLab (version 4)

For manuscripts utilizing custom algorithms or software that are central to the paper but not yet described in the published literature, software must be made available to editors and reviewers upon request. We strongly encourage code deposition in a community repository (e.g. GitHub). [Nature Methods guidance for providing algorithms and software for publication](#) provides further information on this topic.

► Materials and reagents

Policy information about [availability of materials](#)

8. Materials availability

Indicate whether there are restrictions on availability of unique materials or if these materials are only available for distribution by a for-profit company.

No unique materials were used.

9. Antibodies

Describe the antibodies used and how they were validated for use in the system under study (i.e. assay and species).

Clone numbers of antibodies are included. Antibodies used were validated from the purchased company (BD, ebiosciences or Biogend) against murine or human use.

10. Eukaryotic cell lines

a. State the source of each eukaryotic cell line used.

The eukaryotic cell lines YAC-1, K562 and B16-F10 were purchased from the American Type Culture Collection

b. Describe the method of cell line authentication used.

None of the cell lines used have been authenticated.

c. Report whether the cell lines were tested for mycoplasma contamination.

The cell lines were not tested for mycoplasma contamination.

d. If any of the cell lines used are listed in the database of commonly misidentified cell lines maintained by [ICLAC](#), provide a scientific rationale for their use.

No commonly misidentified cell line was used

► Animals and human research participants

Policy information about [studies involving animals](#); when reporting animal research, follow the [ARRIVE guidelines](#)

11. Description of research animals

Provide details on animals and/or animal-derived materials used in the study.

As stated in Materials:
Male and female tamox-cre mice:(Gt(ROSA)26Sortm2(cre/ERT2)Brn/Cnrm)21 mice
Male and female scap floxed mice:(B6;129-Scaptm1Mbjg/J)48
Male C57BL/6J mice were purchased from Harlan or breed in house
All mice were used between 6 and 20 weeks of age.

Policy information about [studies involving human research participants](#)

12. Description of human research participants

Describe the covariate-relevant population characteristics of the human research participants.

Blood samples were obtained from normal healthy donors from whom written consent had been obtained. Ethics was granted by the local research ethics committee.

Flow Cytometry Reporting Summary

Form fields will expand as needed. Please do not leave fields blank.

▶ Data presentation

For all flow cytometry data, confirm that:

- 1. The axis labels state the marker and fluorochrome used (e.g. CD4-FITC).
- 2. The axis scales are clearly visible. Include numbers along axes only for bottom left plot of group (a 'group' is an analysis of identical markers).
- 3. All plots are contour plots with outliers or pseudocolor plots.
- 4. A numerical value for number of cells or percentage (with statistics) is provided.

▶ Methodological details

5. Describe the sample preparation.
- For mouse NK cell culture splenocytes were isolated from the murine spleen and cultured in IL-15 (10 ng/ml , Peprotech; in RPMI media) for 6 days. The mouse splenocytes were re-fed with IL-15 (10 ng/ml , Peprotech; in RPMI media) on day 4 of culture.
For T cell culture, splenocytes were isolated from murine spleen and T cells were activated with anti-CD3 (2c11, 500 ng/ml) and IL-2 (20 ng/ml, NCI preclinical repository) in RPMI media for 36 h at 10×10^6 cells/ml. Following activation, cells were washed and maintained in IL-2 (20 ng/ml). Cells were re-fed IL-2 (20 ng/ml) and the cell concentration adjusted to 0.3×10^6 cells/ml every 24 h for a further 5 days.
Blood samples were obtained from normal healthy donors. PBMCs were isolated by Lymphoprep (Axis-Shield) gradient.
6. Identify the instrument used for data collection.
- BD FACSCanto II, BD LSRFortessa and BD FACSCalibur
7. Describe the software used to collect and analyze the flow cytometry data.
- FACS DIVA software was used for collecting the flow cytometry data. FlowJo software was used for analysis of the raw data.
8. Describe the abundance of the relevant cell populations within post-sort fractions.
- No cell sorting performing.
9. Describe the gating strategy used.
- Live cells were gated according to their forward scatter (FSC-A) and side scatter (SSC-A), single cells according to their FSC-W and FSC-A and NK cells were identified as NK1.1+, NKp46+ and CD3- cells for murine NK cells and CD56+/CD3- for human NK cells

Tick this box to confirm that a figure exemplifying the gating strategy is provided in the Supplementary Information.